RESEARCH   **Open Access**

Comparative evaluation of cigarette smoke and a heated tobacco product on microglial toxicity, oxidative stress and inflammatory response

Alfio Distefano[1], Laura Orlando[1], Konstantinos Partsinevelos[1], Lucia Longhitano[1], Rosalia Emma[2,3], Massimo Caruso[1,3,4], Nunzio Vicario[1], Simona Denaro[1], Ang Sun[4,5], Antonio Giordano[4,5], Barbara Tomasello[6], Amer M. Alanazi[7], Giovanni Li Volti[1,3]* and Angela Maria Amorini[1]

Abstract

Background Tobacco smoking is the leading cause of preventable death and disease worldwide, with over 8 million annual deaths attributed to cigarette smoking. This study investigates the impact of cigarette smoke and heated tobacco products (HTPs) on microglial function, focusing on toxicological profiles, inflammatory responses, and oxidative stress using ISO standard and clinically relevant conditions of exposure.

Methods We assessed cell viability, reactive oxygen species (ROS) production, lipid peroxidation, mitochondrial function, unfolded protein response, and inflammation in human microglial cells (HMC3) exposed to cigarette smoke, HTP aerosol or nicotine.

Results Our findings show that cigarette smoke significantly reduces microglial viability, increases ROS formation, induces lipid peroxidation, and reduces intracellular glutathione levels. Cigarette smoke also alters the expression of genes involved in mitochondrial dynamics and biogenesis, leading to mitochondrial dysfunction. Additionally, cigarette smoke impairs the unfolded protein response, activates the NF-κB pathway, and induces a pro-inflammatory state characterized by increased TNF and IL-18 expression. Furthermore, cigarette smoke causes DNA damage and decreases the expression of the aging marker Klotho β. In contrast, HTP, exhibited a lesser degree of microglial toxicity, with reduced ROS production, lipid peroxidation, and mitochondrial dysfunction compared to conventional cigarettes.

Conclusion These results highlight the differential toxicological profile of cigarette smoke and HTP on microglial cells, suggesting a potential harm reduction strategy for neurodegenerative disease for smokers unwilling or unable to quit.

Keywords Microglia, Cigarette smoking, Nicotine, Heated tobacco product, Toxicity, Oxidative stress, Inflammation, Aging

*Correspondence:
Giovanni Li Volti
livolti@unict.it
Full list of author information is available at the end of the article

Introduction

Tobacco smoking stands as the foremost cause of preventable death and disease globally [1]. With an estimated 1.3 billion smokers worldwide, cigarette smoking alone claims over 8 million lives annually. On average, smokers sacrifice at least 10 years of life expectancy compared to non-smokers and endure a significant decline in quality of life [2, 3]. Moreover, smoking exerts a profound negative influence on neurocognitive and neuropathological conditions, exacerbating anxiety, cognitive decline, and increasing the risk of Alzheimer's disease (AD) and stroke, albeit displaying a protective effect against Parkinson's disease [4–9]. To this regard, epidemiological studies have shown that cigarette smoking is an important risk factor of cognitive decline and AD, the most common form of dementia [1–3]. Cigarette smoking not just doubles the risk of developing dementia and AD [10], it also accelerates the rate of cognitive decline in elderly without dementia [2]. In addition, cigarette smoking has been known as an important environmental aging accelerator [11, 12] partly because it induces oxidative stress in multiple organs including the brain [4, 13, 14]. Previous studies showed that during the combustion of a cigarette, more than 4000 chemicals are produced, many of whom are reactive radicals, leading to a defective cellular signaling and accumulation of malfunctioned proteins [5]. Previous studies suggest that smoking habit shows deleterious neurological effects via oxidative stress, triggering inflammation via a cytokine-mediated immune response with the release of pro-inflammatory mediators such as TNF, and interleukins that may exert neurotoxic effects accelerating brain aging. Consistently, a number of reports have shown that oxidative stress was found in the brains of cigarette smoke exposed-animals [6, 7]. However, although these studies suggest a linkage between cigarette smoking and cognitive impairment, there is insufficient experimental data demonstrating how smoking induces cognition-related pathological changes. To this regard, previous studies suggested the potential involvement of non-neuronal cell types such as microglia, as active players in such complex pathophysiological processes leading to brain injury [15].

Microglia are highly specialized resident immune cells, which act as the brain's homeostatic sensor. Cigarette smoke detrimentally impacts microglia through direct and indirect pathways, triggering inflammatory responses and functional impairments [16]. Different studies demonstrated that toxicants in smoke promote oxidative stress and neuroinflammation, impair phagocytosis, disrupt intercellular communication exacerbating neurodegeneration [16]. However, one of the limits of these studies was the use of not clinically relevant exposure conditions with particular regard to nicotine concentration or poor standardization of methods. Finally, no studies are currently available on the comparison of the neurotoxicological profiles of cigarettes vs. heated tobacco products (HTPs) in order to elucidate and potentially offering a possible alternative for those smokers who are not willing or are not able to quit smoking.

The present in vitro study aims to assess and compare the impact of cigarette smoke and HTPs aerosol on microglial function with particular regard to toxicological profile, inflammatory response, and oxidative stress in clinically relevant conditions.

Materials and methods

Cell culture

The transformed human microglial cells (HMC3) (ATCC CRL-3304) were established through SV40-dependent immortalization of a human fetal brain-derived primary microglia culture. They retain the properties of primary microglial cells and represent homogeneous cell populations which can be grown indefinitely and might represent a convenient system for the biochemical analysis of microglial cells functions. The HMC3 cells were cultured with EMEM medium (SIGMA® M4655™) added with 10% FBS (ATCC® 30-2020™), Sodium pyruvate 1% (Sigma® S8636), 1% MEM Non-Essential Amino Acids (GIBCO® 11140-50), and 1% Antibiotic-Antimycotic (15240062, Invitrogen™ Thermo Fisher Scientific).

Test products and exposure of cells to smoke/aerosol

For the exposure of microglial cells to smoke or aerosol were used a standardized tobacco reference cigarette, 1R6F (Center of Tobacco Reference Products, University of Kentucky), and an HTP commercially available, IQOS 3 DUO (referred subsequently as IQOS; Philip Morris International, Neuchâtel, Switzerland), respectively. The tobacco consumables used with IQOS were the Heat-Sticks (or Heets) "Sienna selection" (Red). All IQOS devices and consumables were purchased from authorized dealers in Italy.

Preparation of smoke and aerosol aqueous extracts (AqE)

For the 1R6F cigarette smoke exposure was used the Borgwaldt LM1 smoking machine (Borgwaldt KC GmbH). The LM1 is a linear one-port mechanical syringe-based smoking machine that performs a whole smoke exposure [17].

The 1R6F reference cigarettes were conditioned before use for a minimum of 48 h at 22±1 °C and 60±3% relative humidity in a climatic chamber (Memmert, HCP105), in accordance with ISO 3402:1999 [18]. Then, 1R6F were smoked following the Health Canada Intense (HCI) regimen (55 mL puff volume, 2 s puff duration, 30 s puff frequency, with bell shaped profile and the hole vents blocked), accredited under ISO/TR 19478-2:2015 [19].

IQOS devices were used according to the manufacturer's instructions. They were fully charged, cleaned, and loaded with fresh tobacco consumables before each exposure. For the IQOS aerosol exposure was used the Borgwaldt LM4E vaping machine (Borgwaldt KC GmbH). The LM4E is a linear 4-port machine with one piston pump that delivers undiluted aerosol [20]. IQOS system was vaped following a modified Health Canada Intense (mHCI) regimen (55 mL puff volume, 2 s puff duration, 30 s puff frequency, with bell shaped profile, but with filter vents unblocked to avoid device overheating). IQOS system was manually button-activated 30 s before each puffing session to initiate device heating prior to syringe activation.

HMC3 cells were exposed to aqueous extract (AqE) generated by bubbling 1R6F smoke (6 cigarettes with 9 puffs/cigarette; total 54 puffs in 30 ml PBS) or IQOS aerosol (10 sticks with 12 puffs/stick; total 120 puffs in 40 ml PBS) in ice-cold impinger.

Quantification of nicotine in HPLC

Nicotine identification and quantification in AqE was conducted using reversed phase chromatographic technique. The apparatus consisted in a SpectraSystem P4000 pump connected to a highly sensitive UV6000LP diode array detector (ThermoQuest Italia, Rodano, Milan, Italy), equipped with a 5-cm-light-path flow cell and set up between 190 and 300 nm wavelength. Puffs from different sources of nicotine (1.8 puffs for 1R6F or 3 puffs for IQOS, respectively) were bubbled in 1 ml PBS which was then loaded onto a 150×4.6 mm, 3 µm particle size Hypersil Gold RP C18 column provided with its own guard column (Thermo Fisher Scientific, Milan, Italy). A binary gradient was built up using buffers A (10% methanol+90% 10mM KH_2PO_4 pH 7.4) and B (50% methanol+50% 10mM KH_2PO_4 pH 7.4) mixed in the following linear steps: 0–5 minutes 100% A, 5–30 minutes 100% B. Flow rate was 1 ml/min and column temperature was kept at 30°C. The nicotine peak was eluted with a k' = 13 (where k' = V - V_0/V_0, with V=the elution volume of the compound of interest and V_0=the void volume of the system) and its quantification was performed at its maximum of absorbance (λ=268 nm) [21].

Nicotine solution preparation

Nicotine (SIGMA® N3876™) was used as a reference standard for our experiments. The nicotine standard was diluted in the culture medium to a concentration of 340 nM established after calculating the IC_{50} of HMC3 cells.

MTT assay and IC50 evaluation

Cytotoxicity evaluation was performed through MTT assay to establish the IC_{50} of cells exposed to 1R6F aqueous extract (AqE).

Briefly, HMC3 cells were seeded in a 96-well plate at a density of $10×10^3$ cells/well. After 24 h they were exposed to AqE at different nicotine concentrations (0.067 nM=$4.3×10^{-7}$ puffs/ml; 0.27 nM=$1.7×10^{-6}$ puffs/ml; 2.2 nM=$1.4×10^{-5}$ puffs/ml; 17 nM=$1.11×10^{-4}$ puffs/ml; 34 nM=$2.2×10^{-4}$ puffs/ml; 140 nM=$8.8×10^{-4}$ puffs/ml; 1100 nM=$7×10^{-3}$ puffs/ml; 2200 nM=$1.4×10^{-2}$ puffs/ml; $1.76×10^4$ nM=$1.1×10$ puffs; $1.41×10^5$ nM=0.9 puffs). Exposure of cells to AqE was maintained for 24 h.

Cell viability was measured through the colorimetric tetrazolium salts assay. This assay evaluates total cellular integrity and assesses the ability of cells to reduce, by means of the mitochondrial succinate dehydrogenase, 3-(4,5-dimethylthiazol-2-yl)-2,5-diphenyl tetrazolium bromide (MTT). The tetrazolium salts enter the cells and are transformed into violet-coloured formazan crystals. The level of formazan is used as an indirect index of cell density. After incubating the cells for 3 h, in 5% CO_2 at 37 °C, with 100 µl of the tetrazolium salt solution (0.5 mg/ml), the supernatant was removed and 100 µl of DMSO per well was added for the elution of the crystals. Eventually, the optical density (OD) was measured at a wavelength of 570 nm with the use of a microplate spectrophotometer (Biotek Synergy H1 multiplate reader, Milan, Italy).

Assessment of cytotoxicity by real-time cell analysis (RTCA)

Real-time cell proliferation analysis was performed using the xCELLigence RTCA DPsystem (Agilent). The background impedance was measured in E-plate 16 with 100 µl medium (without cells) after 30 min incubation period at room temperature. HMC3 cells were detached, counted and seeded in E-16 xCELLigence plate at a density of $5×10^3$ cells/well. Plates were subsequently incubated at 37 °C, 5% CO2 for 30 min to allow cell settling to the bottom of the well. After incubation, cells were treated respectively with nicotine, IQOS AqE and 1R6F AqE at the same concentration of 340 nM. Real-time changes in electrical impedance were measured and expressed as "cell index", defined as (Rn-Rb)/15, where Rb is the background impedance and Rn is the impedance of the well with cells. Cell proliferation was monitored every 20 min for 48 h.

Reactive oxygen species production and lipid peroxidation analysis

Extracellular Reactive Oxygen Species formation (ROS) was determined fluorometrically (Biotek Synergy H1 multiplate reader, Milan, Italy). Briefly, 100 µl of cell supernatant was added to each well of a 96-well microplate (PerkinElmer, Milan, Italy) and dichlorofluorescein diacetate (DCFA-DA) (Sigma Aldrich, Milan, Italy – D6883), was first dissolved in DMSO, and then was

added to a final concentration of 10 μM. Then, the plate was incubated for 1 h in the dark. Thereafter, fluorescence was read with an excitation at 485 nm and emission at 528 nm and, finally, fluorescence intensity was normalized to cell number [22]. Lipid peroxides were examined by C11-BODIPY 581/591 (BODIPY) staining. Briefly, at the end of treatment, cells were incubated with BODIPY at a final concentration of 5 μM for 30 min at 37 °C in the dark. Then, the washed cells were analyzed via flow cytometry to determine the intensity of green fluorescence, which was positively correlated with the level of lipid peroxides.

Assessment of mitochondrial potential, mass and fragmentation

Mitochondria were stained with 200 nM MitoTracker Red CMXRos probe (ThermoFisher Scientific, Milan, Italy) for 30 min at 37 °C, according to the manufacturer's instructions. MitoTracker deep Red is a red-fluorescent dye that stains mitochondria in live cells and accumulates selectively in mitochondria due to its negative membrane potential. The dye is chemically reactive linking to thiol groups in the mitochondria, becomes permanently bound, and thus remains after the cell death or fixation [23, 24]. Briefly, the cells were seeded in a 96-well plate (Cell Carrier Ultra) at a density of 10×10^3 cells. After 24 h HMC3 cells were treated with nicotine or IQOS AqE or 1R6F AqE at the same concentration of 340 nM for 6 and 24 h. Following these two different time points, cells were stained with MitoTracker and then washed 3 times in phosphate-buffered saline (PBS) to remove the unbound probe. Nuclei were stained by NucBlue™ Live ReadyProbesTM Reagent (R37605) for 10 min at 37 °C, according to the manufacturer's instructions, and washed 3 times in PBS.

Operetta (PerkinElmer, MA, USA) was used for image acquisition, where cells were maintained at 37 °C. Data collected were analyzed by Harmony software (Version number 4.9; PerkinElmer, MA, USA). All experiments were performed in quadruplicate and the results were analyzed by statistical analysis.

Real-time PCR for gene expression analysis

HMC3 cells were seeded in T-25 flasks. When they reached confluence at 80%, they were treated with nicotine or IQOS AqE or 1R6F AqE for 6 h. Next, RNA was extracted using Trizol® reagent (Invitrogen, Carlsbad, CA, USA).First-strand complementary DNA (cDNA) was then synthesized with a reverse transcription reagent from Applied Biosystems (Foster City, CA, USA). Quantitative real-time PCR (qRT-PCR) was performed with the use of Rotor Gene Q Real-Time PCR System (QIAGEN) by employing the SYBR Green PCR MasterMix (Life Technologies, Monza, Italy). The specific PCR products were detected by SYBR green fluorescence. The relative messenger RNA (mRNA) expression level was calculated by the threshold cycle (Ct) value of each PCR product and normalized with that of β-actin using a comparative $2^{-\Delta\Delta Ct}$ method Table 1.

Western blot analysis

For western blot analysis, cells were seeded in T-25 flasks at a final density of 1×10^6 for each flask and incubated at 37 °C before exposure. Nicotine or IQOS AqE or 1R6F AqE was added at the final concentration of 340 nM on cells and incubated for 24 h. Then, cells were washed in PBS, detached using a cell culture Tripsin-EDTA solution 0.25% −0.2 g EDTA (Sigma -Aldrich T4049) and centrifuged for 5 min at 300 x g to collect dry pellet, which were stored at −80 °C until use. Proteins were extracted mechanically by sonication (3 cycles for 10 s at 4 °C) in 100 μl of PBS supplemented with protease inhibitor (1:100, Cat#P8340, Merck). Samples were centrifuged at 13,000 rpm for 10 min at 4 °C.

Briefly, for Western blot analysis, 30 μg of proteins were loaded onto a 12% poly-acrylamide gel Mini-PROTEAN® TGX™ (BIO-RAD, Milan, Italy). Electro-transfer to nitrocellulose membrane was obtained through Trans-Blot® TurboTM (BIO-RAD) using a Trans-Blot® SE Semi-Dry Transfer Cell (BIO-RAD). Membranes were blocked in Blocking Buffer (Biorad Cat #12010020), according to the manufacturer's protocol. After blocking, membranes were incubated with antibodies against IRE1α (Inositol

Table 1 Primer sequences for gene expression analysis

Genes	Forward Primer (5′−→3′)	Reverse Primer (5′−→3′)
MFN1	TCGGGAAGATGAGGCAGTTT	TGCCATTATGCTAAGTCTCCG
MFN2	CGGGAAGGTGAAGCGCAATG	ACCAGGAAGCTGGTACAACG
OPA1	GAAAGGAGCTCATCTGTTTGGAGTC	TTCTTCCGGAGAACCAAAATCG
FIS1	ACTACCGGCTCAAGGAATACG	CATGCCCACGAGTCCATCTT
SIRT1	AGGCCACGGATAGGTCCATA	GTGGAGGTATTGTTTCCGGC
HMOX1	TGTTGGAGCCACTCTGTTCC	GCTCAAAAACCACCCCAACC
IL-18	GATAGCCAGCCTAGAGGTATGG	CCTTGATGTTATCAGGAGGATTCA
TNF	GCAACAAGACCACCACTTCG	GATCAAAGCTGTAGGCCCCA
DRP1	GTGGGCGGGACCACGATGAG	AATGGGCTCTCCAAAAACTA
β-actin	ACGTTGCTATCCAGGCTGTGCTAT	TTAATGTCACGCACGATTTCCCGC

requiring enzyme-1 α) (1:500, ab189494, ABCAM), HSP90 (heat shock protein 90) (1:500, ab203085, ABCAM), HSP60 (heat shock protein 60) (1:500, ab190828), CLPP (Caseinolytic Mitochondrial Matrix Peptidase Proteolytic Subunit) (1:500, Cat #PA5-52722, Invitrogen), BIP (Binding Immunoglobulin Protein) (1:1000, cell signaling 3177T), BAX (bcl-2-like protein 4) (1:1000, cell signaling 2772T), PERK (Protein Kinase RNA-Like ER Kinase) (1:1000, cell signaling 5683T) and HO-1 (heme oxygenase 1) (1:1000, ab52947, ABCAM), overnight at 4 °C. The next day, membranes were washed three times in PBS tween 0.1% for 5 min and incubated with anti-rabbit IRDye700CW secondary antibodies (1:5000) in blocking solution for 1 h at room temperature. All the antibodies were diluted in Odyssey Blocking Buffer. The obtained blots were visualized by an Odyssey Infrared Imaging Scanner (Licor, Milan, Italy). Densitometric analysis was used for protein level quantification, normalizing data to protein levels of β-actin.

Immunocytochemical analysis

Briefly, HMC3 cells were detached and seeded in a 96-well plate (Cell carrier ultra) at a density of 10×10^3 cells/well. After 24 h, cells were treated with nicotine or IQOS AqE or 1R6F AqE at the same concentration of 340 nM for 6 and 24 h.

After washing with PBS, cells were fixed in 4% paraformaldehyde (category no. 1004968350 Sigma-Aldrich, Milan, Italy) for 20 min at room temperature. Subsequently, cells were incubated with human NRF2 (nuclear factor erythroid 2-related factor 2) antibody (ab 62352, ABCAM), at a dilution of 1:100, human Nf-kB (nuclear factor kappa-light-chain-enhancer of activated B cells) antibody (GTX 107678) at a dilution of 4,4 μg/ml overnight at 4 °C. The next day, cells were washed three times in PBS for 5 min and the nuclei were stained by DAPI (1 μg/ml) (27706074, Thermo Fisher Scientific, Milan, Italy) for 1–5 min at 37 °C, according to the manufacturer's instructions. The fluorescent images were obtained using Operetta (PerkinElmer, MA, USA).

DNA damage assessment by comet assay

Neutral Single cell gel electrophoresis assay (comet assay) was carried out as previously described [25] with slight modifications in order to detect double strand breaks on nuclear DNA. Briefly, HMC3 were treated for 24 h as described above. After treatments, cells were trypsinized and resuspended in cold PBS Ca^{2+}/Mg^{2+} free.

Then, each cell sample was homogenized with 0.7% low melting point agarose solution and dropped onto Trevigen® treated slides, allowing their jellification. Next, slides were immediately immersed in a lysis buffer (R&D System) and incubated 1 h at 4 °C. Then, all slides were transferred to an electrophoresis tank and covered with a cold neutral buffer (90 mM Tris-base, 90 mM boric acid, and 2 mM Na2 EDTA, pH 8) incubating 20 min at 4 °C for allowing DNA unwinding. Afterwards, the electrophoresis was carried out for 40 min at 4 °C (0.5 V/cm). Once the electrophoresis finished, the slides were washed twice with a 300mM NaOH solution for 5 min, then neutralized in Tris-buffer (0.4 M Tris-HCl [pH 7.5]) and dehydrated with 70% ethanol. Subsequently, DNA was stained with SYBR Green® (1:10.000 dilution in TE buffer –Tris-HCl 10 mM pH 7.5, EDTA 1 mM) for 20 min at room temperature in darkness. Finally, the slides were air-dried and kept in dark conditions. Comet nucleoids and tails were visualized using a Leica DMI 5500 fluorescence microscope (λexc 490 nm). At least 50 nucleoids were randomly analyzed to determine DNA damage. Images of stained slides were analyzed with Open Comet vs. 13.1. The level of DNA damage of each sample was calculated as Tail Moment (TMOM), defined as the product of the percentage of DNA in the tail of the comet and Tail Length.

Immunofluorescence

Briefly, HMC3 cells were detached and seeded in a Chamber Slide™ (Nunc) at a density of 40×10^3 cells/well. After 24 h, cells were treated with nicotine or IQOS AqE or 1R6F AqE at the same concentration of 340 nM for 24 h.

Immunofluorescence was performed as previously described [26, 27]. Briefly, after washing twice in PBS, cells were stained with CellMask™ Deep Red Plasma Membrane Stains 1X working solution for 10 min at 37 °C, cells were washed three times. Then, cells were fixed in 4% paraformaldehyde for 20 min at room temperature. After fixation, cells were washed three times in PBS for 5 min and treated with a blocking solution (5% FBS and 95% PBS) for 30 min. Subsequently, the cells were washed twice in PBS and incubated with the primary antibody directed against human anti-mouse Klotho β at the concentration of 2 μg/ml (MAB 5889, ReD SYSTEMS) overnight at 4 °C. Then, cells were washed three times in PBS for 5 min and incubated for 1 h with a conjugated secondary antibody: Alexa Fluor® 488 AffiniPure Goat Anti-Mouse IgG (H+L) (Jackson 115-545-003) at dilution 1:500. Nuclei were stained with Hoechst Stain Solution (1:1000, Hoechst 33258, Sigma-Aldrich). The images were captured using a Leica Confocal Microscope TCSSP8 (Leica Microsystems). Ten random visual fields were examined for each condition.

Metabolomic profile by HPLC analysis

After incubation under the different experimental conditions (Untreated, Nicotine, IQOS AqE, 1R6F AqE), cells (3×10^6, $n = 4$ replicates) were washed twice with large volumes of ice-cold PBS and then centrifuged at 1860 x g

Distefano *et al. Journal of Translational Medicine*   (2024) 22:876

Page 6 of 21

for 5 min at 4 °C. Cell pellets were vigorously mixed with 1 mL of ice-cold, nitrogen-saturated, deproteinizing solution (10 mM KH_2PO_4 + HPLC-grade CH_3CN, pH 7.4, 1:3 v: v) and centrifuged at 20,690 x g for 10 min at 4 °C. The supernatants were mixed with two volumes of HPLC-grade chloroform and centrifuged (20,690 x g for 10 min at 4 °C), and the upper aqueous phase was recovered and used for the HPLC analysis of metabolites. The simultaneous separation and quantification of adenine nucleotides (ATP, ADP, and AMP) and nicotinic coenzymes (NAD^+, NADH, $NADP^+$, NADPH) in the protein-free cell extracts were carried out using established HPLC methods [28–31].

Phagocytosis assay

HMC3 cells were seeded in 8-well glass chamber slides (Lab-Tek II, Cat. # 154534) with a density of 3×10^4 cells in 0.5 ml of complete medium per well. Twenty-four hours later, the cells were either treated with complete medium (Untreated) or exposed to 340 nM of nicotine, or IQOS AqE (340 nM), or 1R6F AqE (340 nM) for 24 h. A well without cells was used as a negative control and filled with the complete medium, subsequently treated with the fluorescent latex beads, the blocking buffer, the primary and secondary antibodies, and all the following procedures. After the exposure, cells were treated with fluorescent yellow-green latex beads (Sigma-Aldrich, Cat. # L1030) diluted in pre-warmed EMEM (with 0.05% FBS) to a final concentration of 0.01% [32] for 1 h and 15 min and incubated at 37 °C with 5% CO_2 before they were rinsed by ice-cold PBS five times followed by being fixed by 4% paraformaldehyde (PFA) at room temperature (RT) for 20 min and protected from light. After the fixation, PFA was discarded, and the cells were rinsed with ice-cold PBS five times before proceeding to immunofluorescence assay. The HMC3 cell body was stained by an immunofluorescence assay performed as previously reported with modifications [33, 34].

Briefly to say, after removing PBS, each well in the chamber slide was filled with 500 μl of 0.1% Triton X-100 in PBS to permeabilize the cells for 10 min at RT. After permeabilization, the cells were rinsed with PBS five times before quenching auto-fluorescence by freshly made 1 mg/ml of $NaBH_4$, dissolved in PBS, for 30 min at room temperature. Then, the cells were rinsed five times with PBS before being rocked with the blocking buffer (5% BSA in PBS) at RT for 1 h. After that, the primary antibody (IBA1 monoclonal antibody, Invitrogen Cat. # MA5-27726, 1:150 diluted with 5% BSA in PBS) was applied to the cells. After rocking the cells with the primary antibody at RT for 1 h, the cells were rinsed with PBST (PBS with 0.01% Triton X-100) five times and incubated with the secondary antibody (1:300 diluted with 5% BSA in PBS, donkey anti-mouse IgG, Alexa 488,

Invitrogen Cat. # A-21202) at RT for 1 h. Finally, the cells were rinsed with PBST five times before the nuclei were counter-stained by DAPI (SlowFade Gold Antifade Mountant with DAPI, Invitrogen, Cat. # S36938).

The mounted slides were examined under an Olympus XI81 fluorescence microscope with a 20X objective lens. The nuclei, latex beads, and the cell bodies that were expressing IBA1 (a marker for microglia cells) were visualized by using DAPI, FITC, or TRITC filters, respectively. For each treatment, pictures were taken from five random fields. The total number of cells, the number of fluorescent latex beads, and the number of cells phagocytosed beads were quantified by using Fiji [35] (version May 30, 2017), a distribution of ImageJ and ImageJ2.

Statistical analysis

All experiments were conducted in quadruplicate. Anderson–Darling normality test was performed to assess data distribution. For continuously distributed data, symmetric distributions were summarized using the mean (and standard deviation, SD), while skewed distributions were summarized using the median (and confidence interval at 95%, CI95%). The IC_{50} values were calculated by fitting a sigmoidal dose–response curve with a variable slope to determine the best fit values of nonlinear regression model. Cell viability, oxidative stress (ROS and LOOH), metabolomic, mitochondrial function, ER stress (NRF2 and NF-kB), Klotho β, western blot, and gene expression data were processed via one-way ANOVA followed by Tukey's post hoc multiple comparison test.

Comparisons of DNA damage data were performed using Kruskal-Wallis test followed by Dunnett's post hoc multiple comparison test.

For phagocytosis assay, confidence intervals of the proportions of cells phagocytosis fluorescent beads to the total number of cells were calculated using the exact method for calculating a confidence interval of a proportion. Odds ratios and p-values from Fisher's exact tests were calculated as well. The p-values were adjusted using the False Discovery Rate (FDR) multiple comparison correction method. The q-value ≤ 0.05 is considered as statistically significant. The confidence interval of the count of cells under the microscope was calculated using the Poisson Distribution confidence interval method. All statistical analyses were performed by Prism 9.0 software (GraphPad Software, San Diego, CA, USA), except for phagocytosis assessment data that were analyzed using R (version 4.3.1). All analyses were considered significant with a p value < 0.05.

Results

Cigarette smoke reduces microglial cell viability

In the first set of preliminary experiments IC_{50} (dose decreasing to 50% cell viability) was calculated through

MTT assay, to establish the optimal concentration to be used for subsequent experiments (Fig. 1A). The established concentration was 0.0023 puffs/ml (Fig. 1B) corresponding to 340 nM of nicotine (Fig. 1C) for the 1R6F reference cigarette smoke.

The effects of Nicotine, IQOS AqE and 1R6F AqE at the same nicotine concentration of 340 nM were evaluated on HMC3 cell viability. The results showed that 1R6F AqE treatment caused a significant decrease in normalized cell index (Fig. 1D) and area under the curve (AUC) (Fig. 1E) compared to control cells, indicating a reduction in cell viability. Furthermore, nicotine and IQOS AqE induced a significant increase in cell proliferation (Fig. 1D-E) compared to cigarette smoke treated cells ($p < 0.0001$) whereas no significant differences were observed when compared to untreated cells.

Cigarette smoke increases ROS formation, lipid peroxidation, nitrosative stress and reduces intracellular reduced glutathione

Oxidative stress and ROS production were assessed fluorometrically after 6 h and 24 h of HMC3 nicotine or IQOS AqE or 1R6F AqE treatment (Biotek Synergy H1 multiplate reader, Milan, Italy). 1R6F AqE treatment led to a strong increase in ROS production in cells ($p < 0.0001$) compared to the Untreated group. On the other hand, nicotine and IQOS AqE did not induce the same ROS content (Fig. 2A). The overproduction of ROS has been associated with oxidative damage inflicted on lipid, DNA and protein. This effect was confirmed by the higher levels of lipid peroxidation (LOOH) observed in the presence of 1R6F AqE (Fig. 2B). In this regard, we measured GSH levels showing that cigarette smoke induced a decrease in GSH levels in cells ($p < 0.005$) compared to Untreated cells. On the contrary, nicotine and IQOS do not show a significant reduction in GSH levels (Fig. 2C). We also assessed nitrite and nitrate levels by HPLC analysis, showing that cigarette smoke increases nitrite and nitrate levels compared to the Untreated and to nicotine ($p < 0.05$), (Fig. 2D).

Expression profile of genes involved in mitochondrial dynamics and mitochondrial biogenesis

To further evaluate the effects of cigarette smoke on mitochondrial function, we analyzed the expression of a panel of genes involved in mitochondrial dynamics and mitochondrial biogenesis.

The treatment with nicotine and IQOS induces a significant decrease in DRP1 (Dynamin 1 Like) (Fig. 3A) relative expression levels of mRNAs ($p < 0.0001$ vs. Untreated), ($p < 0.0003$ vs. Untreated). Also, cigarette smoke shows a significant decrease in the relative expression levels of DRP1 mRNA ($p < 0.05$ vs. Untreated), but not highly significant as those of nicotine and IQOS.

The treatment with nicotine, IQOS and 1R6F showed a significant decrease in OPA1 (Mitochondrial Dynamin Like GTPase) (Fig. 3B) relative expression levels of mRNAs ($p < 0.0001$ vs. Untreated). Similarly, we observed a significant decrease in the FIS1 (fission, Mitochondrial 1) (Fig. 3C) relative expression levels of mRNAs with nicotine ($p < 0.0001$ vs. 1R6F) and IQOS ($p < 0.0001$ vs. 1R6F). On the contrary, treatment with 1R6F induced a significant increase of FIS1 ($p < 0.0001$ vs. Untreated). Treatment of HMC3 cells with cigarette smoke induced an increase in the relative mRNA expression levels of the genes involved in the mitochondrial fusion process MFN1 (Fig. 3D) ($p < 0.05$ vs. Untreated, $p < 0.05$ vs. Nicotine, $p < 0.05$ vs. IQOS) and MFN2 (Fig. 3E) ($p < 0.0001$ vs. Untreated, $p < 0.0001$ vs. Nicotine, $p = 0.0001$ vs. IQOS). The expression of Sirtuin 1 gene (SIRT1) (Fig. 3F) involved in mitochondrial biogenesis was decreased with nicotine ($p = 0.001$ vs. 1R6F) and IQOS treatments ($p = 0.001$ vs. 1R6F), while 1R6F induces a significant increase in SIRT1 expression ($p < 0.01$ vs. Untreated).

Cigarette smoke and mitochondrial fitness

Our data showed that at 6 h and 24 h none of the treatments caused a significant increase in mitochondrial fragmentation (Fig. 4B-C). This figure shows representative images of mitochondria fragmentation in Untreated cells and in cells after treatment with nicotine or IQOS AqE or 1R6F AqE (Fig. 4A). These data suggest that mitochondria would not be affected morphologically. To deepen into the energetic status of HMC3 cells undergoing nicotine or IQOS AqE or 1R6F AqE treatment, we studied the intracellular energy charge, calculated as $[ATP + (0.5 * ADP)]/[(ATP + ADP + AMP)]$ (Fig. 4G) and the level of total triphosphates (ATP + GTP + UTP + CTP) (Fig. 4H), following a very sensitive HPLC method. In both of the two cases, results pictured a suffering state exclusively in 1R6F treated-cells. Suspicion of a mitochondrial dysfunction was suggested by the ratio ATP/ADP, as a measure of cellular phosphorylating capacity. Indeed, cigarette smoke (1R6F) manifested a dramatic decrease of the ratio ($p < 0.01$ vs. Untreated), whereas a slighter modification was detected in IQOS samples ($p < 0.05$ vs. Untreated). In addition, NAD+/NADH ratio (Fig. 4E), key parameter managing the speed of Krebs cycle and the efficiency of oxidative phosphorylation, dropped only in cigarettes treatment ($p < 0.05$ vs. Untreated). Coherently, in the same samples, the reducing potential steeply fell (Fig. 4F) ($p < 0.0001$ vs. Untreated).

Effects on unfolded protein response and ER stress in HMC3 cells

Our data showed that IQOS induced an increase in HSP90 (Fig. 5A-D) ($p < 0.05$) protein expression
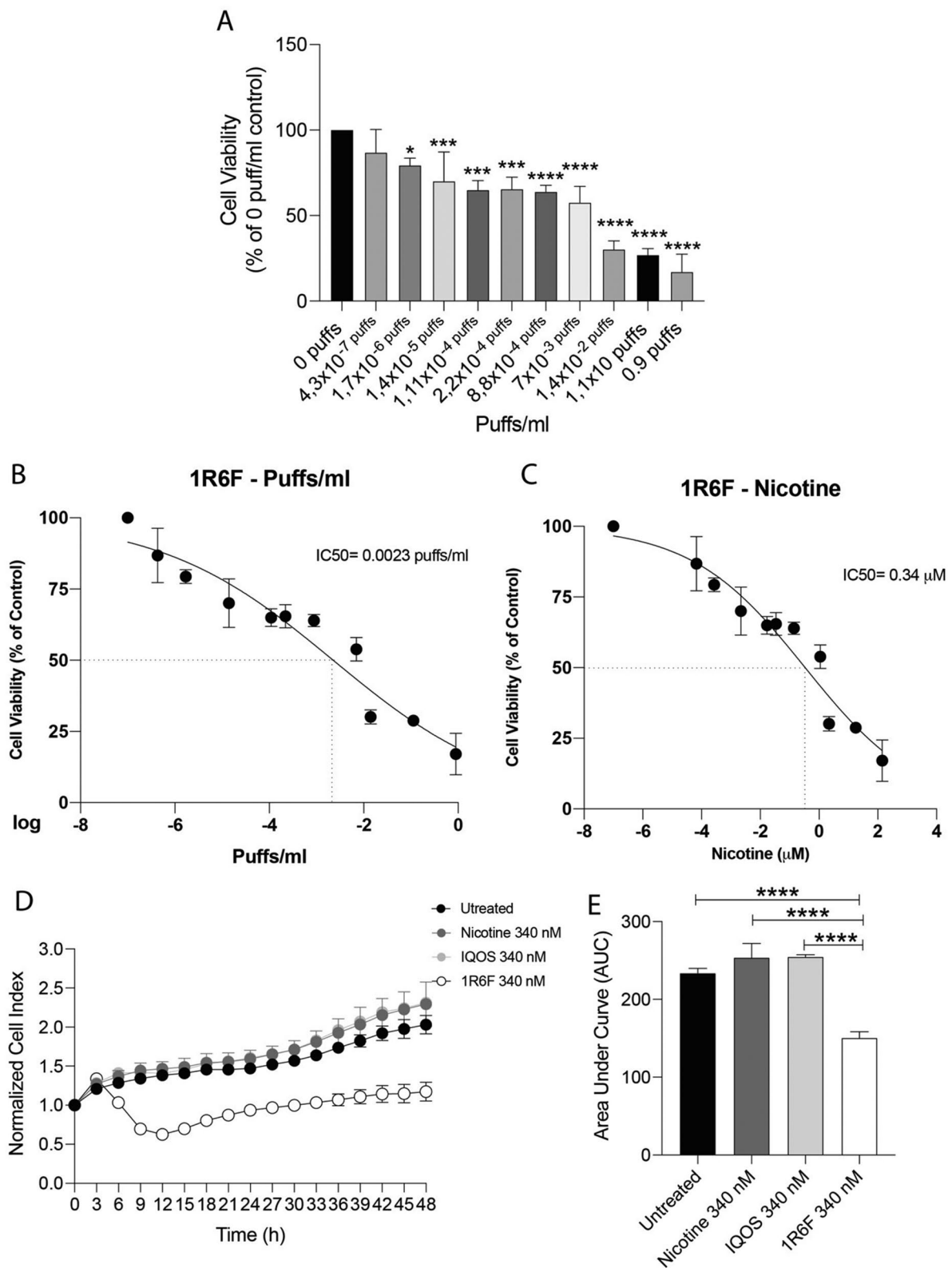
Fig. 1 HMC3 cells viability. (**A**) Cell viability according to bromide 3-(4,5 dimethylthiazol − 2-yl)-2,5-diphenyltetrazolium (MTT) assay after treatment for 24 h at different puffs/ml of cigarette smoke. (**B**-**C**) Inhibition of cell viability (IC$_{50}$). (**D**) Real-time cell proliferation of HMC3 cells after cigarette smoke treatment (normalized cell index). (**E**) Area under curve. All assays were performed in quadruplicate. (*$p < 0.05$, ***$p \leq 0.001$, ****$p \leq 0.0001$)
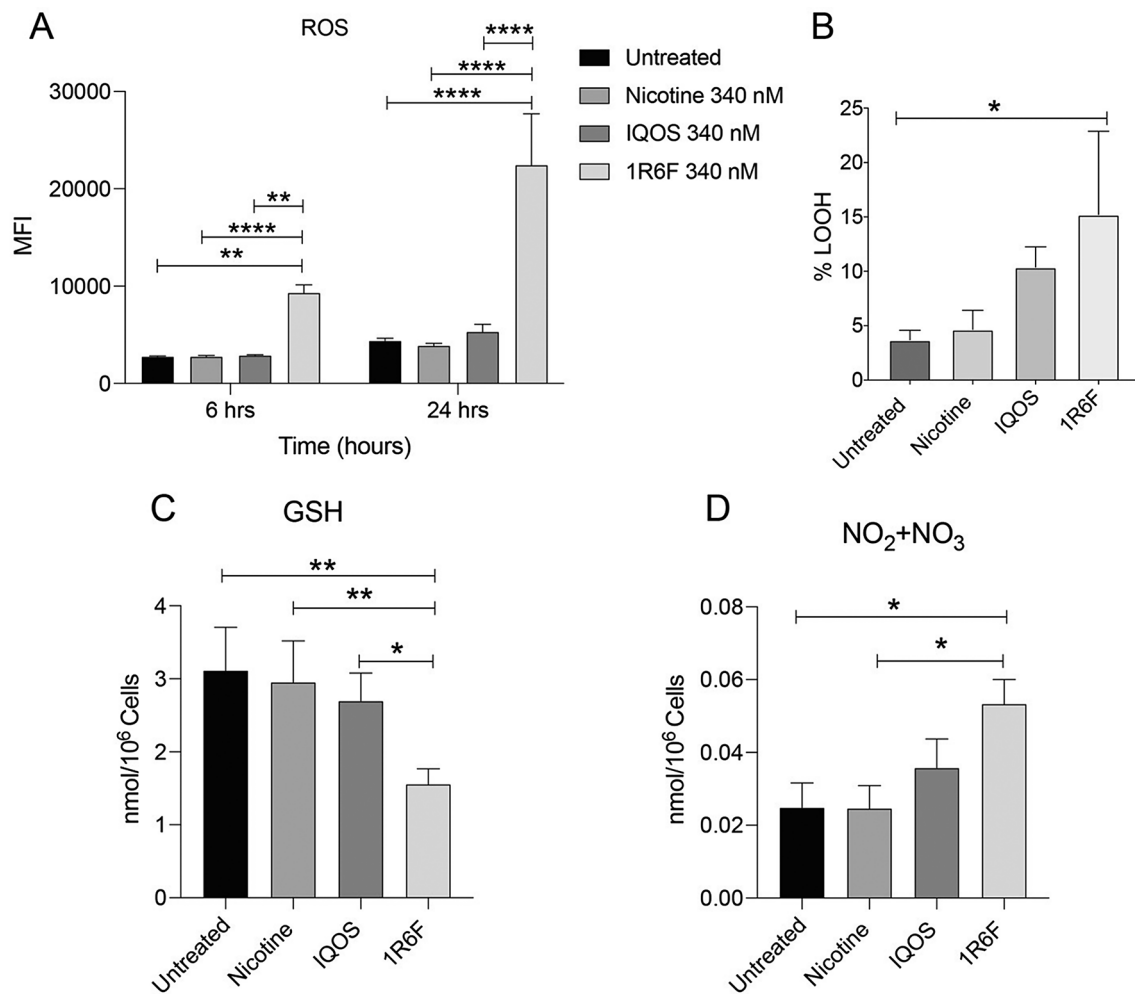
Fig. 2 Effect of cigarette smoke on ROS cell-free production. (**A**) MFI (Mean Fluorescence Intensity) of ROS production after 6 and 24 h of treatment. (**B**) Membrane lipid peroxidation (LOOH) after 24 h of treatment. (**C**) GSH (reduced glutathione) levels after 24 h of treatment evaluated by HPLC analysis. (**D**) Nitrite and Nitrate levels after 24 h of treatment evaluated by HPLC analysis. Data are presented as the mean ± standard deviation of experiment performed in quadruplicate. (*$p < 0.05$; **$p \leq 0.01$; ****$p \leq 0.0001$)

compared to Untreated cells, instead the cigarette smoke showed no variation in HSP90 protein expression. Nicotine induced an increase in HSP60 (Fig. 5B-D) ($p < 0.0001$) protein expression compared to Untraeted cells and, also, the treatment with cigarette smoke ($p < 0.01$) and IQOS ($p < 0.001$) showed an increase in HSP60 protein expression compared to Untreated cells, but less significant. Finally, regarding CLPP (Fig. 5C-D), our data revealed that nicotine induced an increase of protein expression ($p < 0.001$) compared to Untreated cells, while IQOS and 1R6F showed a decrease of the relative protein expression ($p < 0.0001$).

To further study the effects of cigarette smoke on endoplasmatic reticulum (ER) stress, we analyzed the expression of different stress sensors.

Our results showed a significant decrease in IRE1α protein expression following cigarette smoke treatment compared to Untrated cells ($p < 0.001$) (Fig. 6A-E).

Regarding BIP (binding immunoglobulin protein) (Fig. 6B-E), we have found a significant increase following IQOS treatment ($p < 0.001$) and cigarette treatment ($p < 0.001$) compared to controls. As for BAX (Bcl-2Associated X-protein) (Fig. 6C-E) cigarette smoke showed a significant decrease in protein expression compared to Untreated ($p < 0.01$), to nicotine treatment ($p < 0.001$) and also to IQOS treatment ($p < 0.01$. In order to confirm the involvement of unfolded protein response, we also evaluated PERK (protein kinase R (PKR)-like endoplasmic reticulum kinase) (Fig. 6D-E). Our findings showed a significant increase in PERK protein expression following 1R6F treatment compared to Untreated cells ($p < 0.05$).

Cigarette smoke impairs NRF2 translocation and activates NF-kB pathway

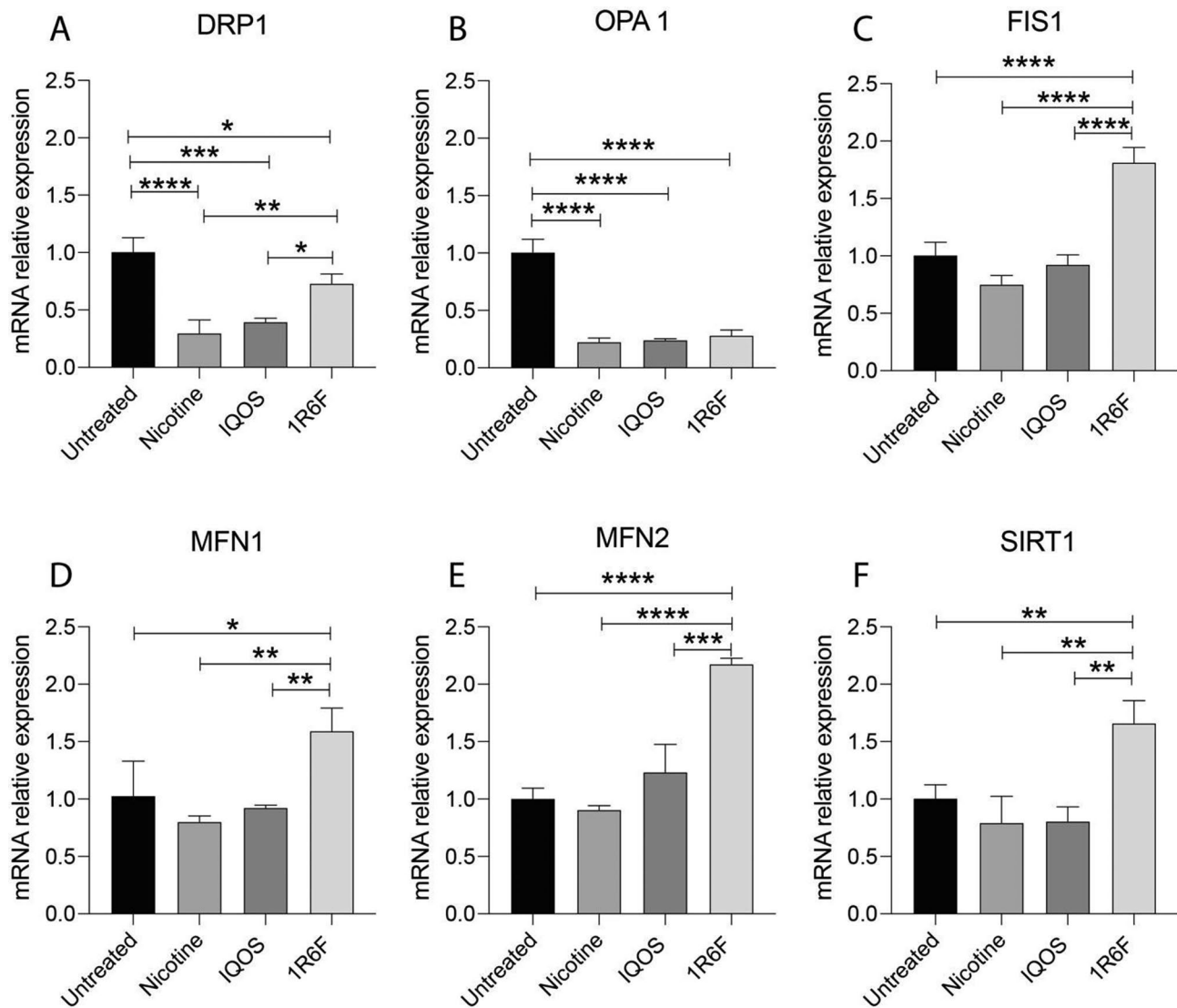Our findings showed that cigarette smoke induces a significant decrease in the percentage of NRF2 (Fig. 7)

Fig. 3 Real-time PCR analysis of genes involved in mitochondrial dynamics and biogenesis. mRNA expression levels of (**A**) DRP1, (**B**), OPA1, (**C**) FIS1, (**D**) MFN1, (**E**) MFN2, (**F**) SIRT1 after 6 h of treatment. Values represent the mean ± SD of experiments performed in quadruplicate. (*$p < 0.05$; **$p \leq 0.01$; ***$p \leq 0.001$; ****$p \leq 0.0001$)

nuclear translocated cells compared to Untreated cells at 6 h ($p < 0.0001$). Furthermore, nicotine and IQOS showed a decrease in the translocation of NRF2 compared to Untreated cells ($p < 0.001$). This decrease relative to NRF2 presence in the nucleus may be associated with the modulation of NRF2-regulated antioxidants genes. The same trend was found at 24 h, however it is not significant at any of the treatments. Consistently, we decided to assess the activation of NF-kB, which is the first regulator of the inflammatory response targeted by NRF2. Our data showed that none of the treatments at 6 h exhibited an increase in the percentage of translocated nuclear NF-κB (Fig. 8). On the other hand, cigarette smoke at 24 h showed an increase in the percentage of NF-κB nuclear

translocated cells compared to nicotine treated cells ($p < 0.01$).

Cigarette smoke impairs the inflammatory state of HMC3 cells

Our results showed that the HO-1 gene expression (Fig. 9A) exhibited a significant.

increase in all treatments compared to the Untreated group ($p < 0.001$ for nicotine, $p < 0.0001$ for IQOS and 1R6F). Furthermore, HO-1 protein expression showed an increase following nicotine treatment (Fig. 9B-C) compared to Untreated cells ($p < 0.01$). Also, IQOS showed an increase of HO-1 protein expression compared to Untreated cells, but it is not significant. On the contrary, cigarette smoke treatment showed a decrease in HO-1
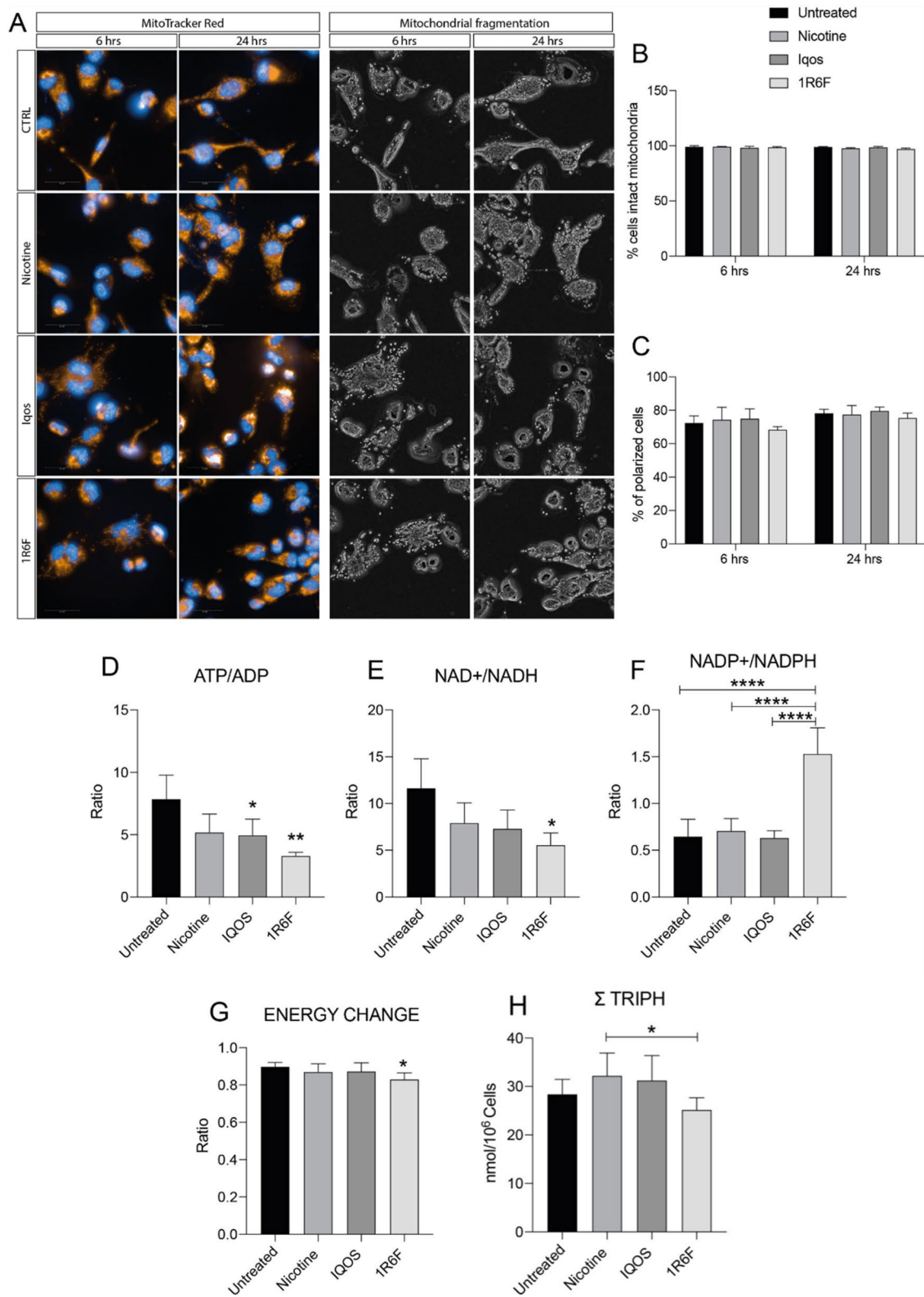
Fig. 4 MitoTraker Red staining (orange color), NucBlue staining (blue color) and metabolic HPLC analysis. (**A**) Computerized analysis of the MitoTracker fluorescence intensity on the Untreated versus Nicotine, IQOS and 1R6F after 6 h and 24 h of treatment. The figures presented are representative of at least three independent experiments. Scale bars in (**A**) 50 μm. (**B**) % cells intact mitochondria. (**C**) % of polarized cells. Effect of nicotine, IQOS and cigarette smoke treatment on levels of major classes of metabolites detected by HPLC (D-H). Values represent the mean±SD of experiments performed in quadruplicate. (*$p < 0.05$, **$p \leq 0.01$, ****$p \leq 0.0001$)
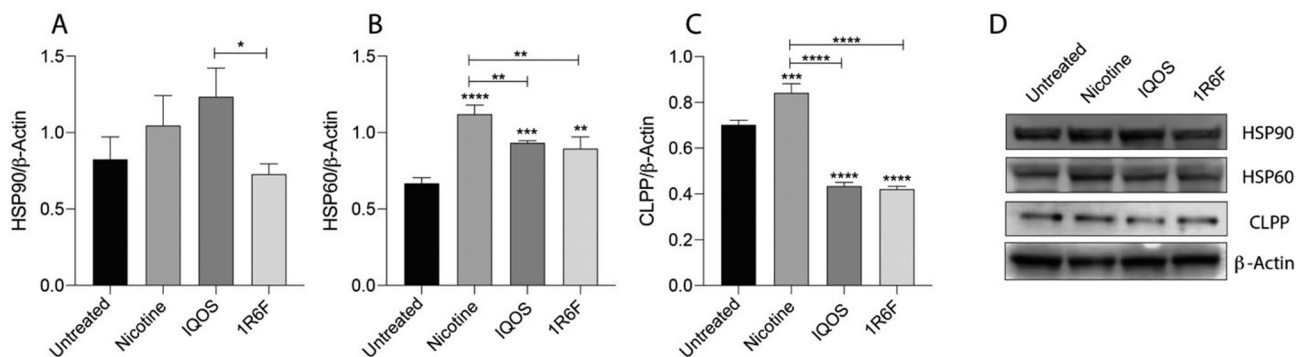
Fig. 5 Unfolded protein response in HMC3 cells. (**A**) Densitometry analysis of HSP90. (**B**) Densitometry analysis of HSP60. (**C**) Densitometry analysis of CLPP. (**D**) Western blot analysis of HSP90, HSP60 and CLPP proteins. β-Actin protein was used as a total protein loading reference. Values represent the mean ± SD of experiments performed in quadruplicate. (*$p < 0.05$, **$p \leq 0.01$, ***$p \leq 0.001$, ****$p \leq 0.0001$)
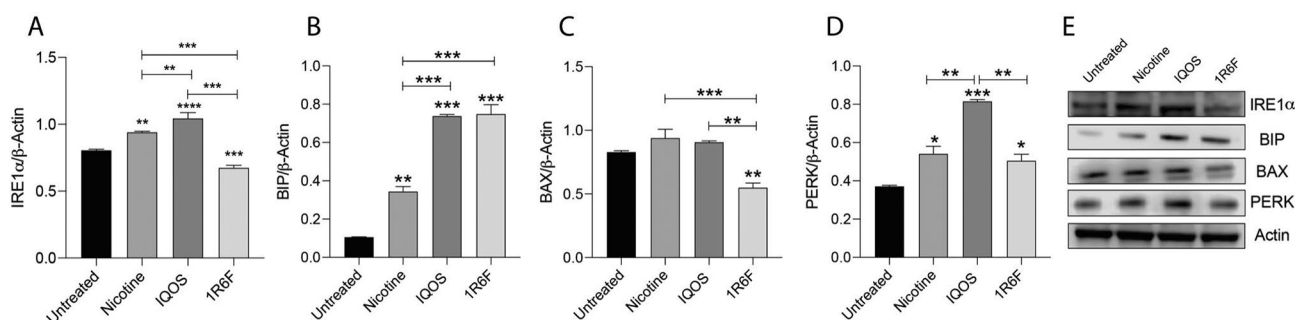

Fig. 6 Effect of HMC3 cells on endoplasmic reticulum (ER) stress. Protein expression levels of (**A**) IRE1α, (**B**) BIP, (**C**) BAX, (**D**) PERK. (**A**) Densitometry analysis of IRE1α. (**B**) Densitometry analysis of BIP. (**C**) Densitometry analysis of BAX. (**D**)Densitometry analysis of PERK. (**E**) Western blot analysis of IRE1α, BIP, BAX, and PERK proteins. β-Actin protein was used as a total protein loading reference. Values represent the mean ± SD of experiments performed in quadruplicate. (*$p < 0.05$, **$p \leq 0.01$, ***$p \leq 0.001$, ****$p \leq 0.0001$)

protein expression (Fig. 9B-C) compared to Untreated ($p < 0.01$). Nicotine and IQOS showed a significant increase of TNF gene expression (Fig. 9D) compared to Untreated cells ($p < 0.0001$). Also, cigarette smoke showed an increase of TNF gene expression ($p < 0.05$), but less significant. Regarding IL-18 gene expression (Fig. 9E), 1R6F treatment showed an increase compared to Untreated cells ($p < 0.05$). Instead, nicotine and IQOS induced a decrease in the relative mRNA expression levels of IL-18 ($p < 0.01$) compared to 1R6F cigarette smoke.

Cigarette smoke induces microglial DNA damage and senescence

Consistently, comet assay (Fig. 10A-B), a well-established marker of DNA damage, showed that the DNA damage of 1R6F treated HMC3 cells at 24 h was higher compared to that of Untreated cells ($p < 0.0001$) and nicotine ($p < 0.0001$) or IQOS treated cells ($p < 0.001$), suggesting the induction of double strand breaks (DSBs) after 1R6F treatment. However, the increase in tail moment (TMOM) observed upon standard cigarette exposure is associated with a slight double-stranded damage, consistent with the doses administered in the treatments. The levels of DSBs were also significantly increased in

IQOS-treated cells, but the extent of damage was negligible and much lower than 1R6F treatment.

In the same way, regarding Klotho β (Fig. 11A, B), which appears to play a key role in slowing aging, nicotine and IQOS treatments had no effect in Klotho β expression compared to Untreated. Conversely, cigarette smoke led to a decrease in the protein expression of Klotho β compared with Untreated ($p < 0.01$).

Phagocytosis assay

Consistently, phagocytosis assay (Fig. 12; Table 2), show that IQOS at 24 h of treatment increase phagocytosis in a significant manner ($p < 0.001$) (Table 3) compared to 1R6F treated cells and ($p < 0.05$) to nicotine treatment.

Compared with untreated cells, cell counts summarized in Table 2 show that all the other treatments, which have the same concentration of nicotine, have relatively higher cell counts (Poisson CIs comparisons), indicating that nicotine stimulates the cell growth and proliferation of HMC3. The pure nicotine treatment shows a similar effect on cell growth to 1R6F cigarette smoke-bubbled PBS treatments. It is interesting to notice that the heated tobacco product IQOS stimulates cell growth to a lesser extent than nicotine or 1R6F, indicating that the other
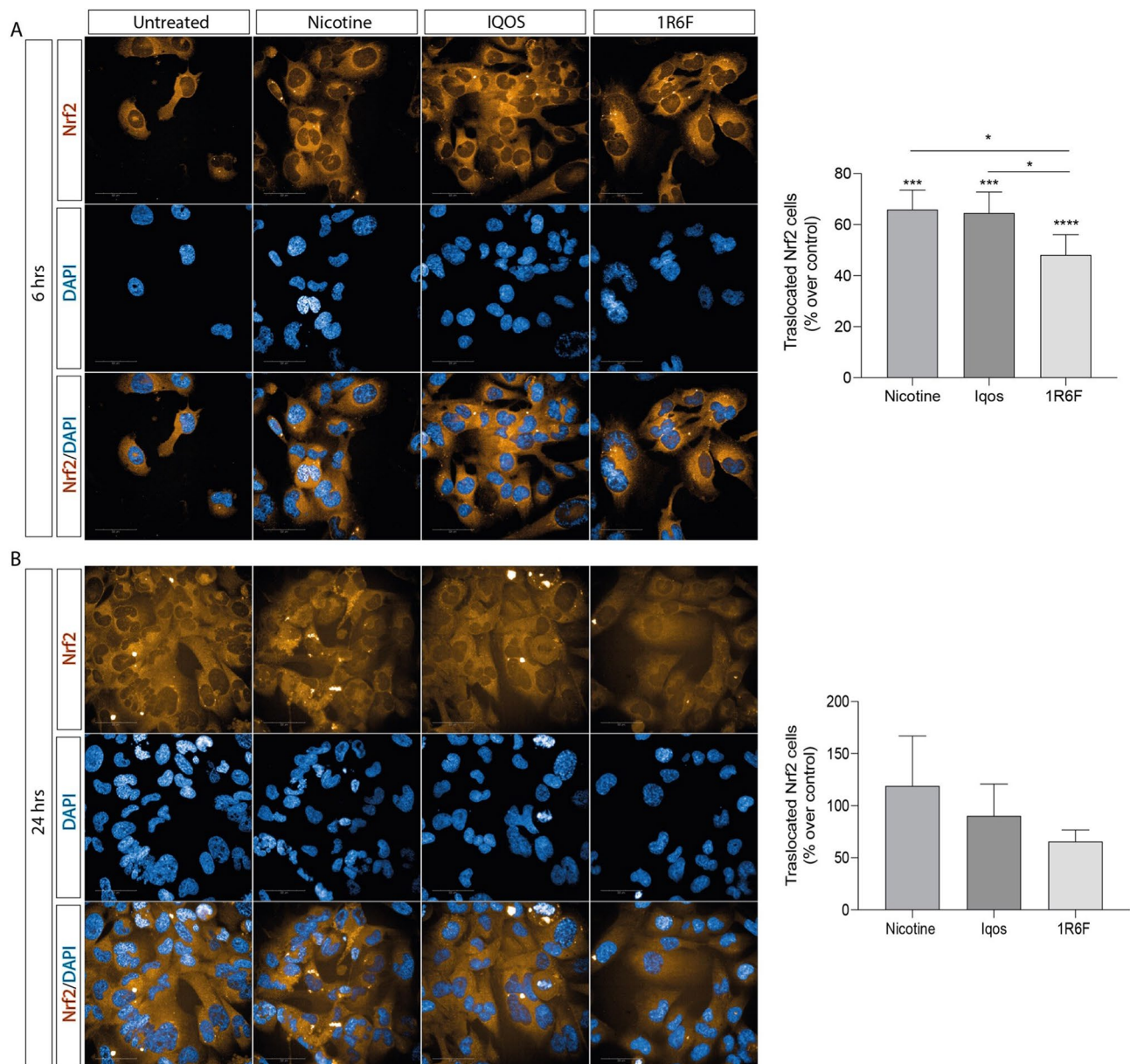
Fig. 7 Effect of cigarette smoke on NRF2 expression. (**A**) Immunocytochemistry for NRF2 at 6 h. (**B**) Immunocytochemistry for NRF2 at 24 h. Values represent the mean ± SD of experiments performed in quadruplicate. (*$p < 0.05$, ***$p \leq 0.001$, ****$p \leq 0.0001$). (Scale bar: 50 μm)

components in the IQOS may have a counter effect on cell growth and worth further investigation.

Discussion

The present in vitro study describes the comparison of the toxicological profiles of nicotine, a commercially available HTP, and conventional cigarettes on microglia using standard and clinically relevant conditions. Our findings reveal distinct characteristics exhibited by microglia in response to various smoke exposure stimuli, encompassing cellular responses and metabolic states. These results enrich and deepen our comprehension of microglial metabolic changes in the context of

inflammatory responses [36]. Previous reports showed that in smokers, the maximal total brain nicotine concentrations can be calculated as 40 nM after a single puff and 357 nM after smoking an entire cigarette. We showed that under our experimental conditions, and the use of 340 nM nicotine concentration in nicotine, IQOS AqE and 1R6F AqE treatments, nicotine and HTP did not reveal significant toxicity in comparison to Untreated condition, whereas combustible cigarette exhibited a time dependent significant decrease in cell viability. These results are consistent with the suggestion that toxicity may be dependent on combustion products rather than the direct effect of nicotine. Furthermore, our
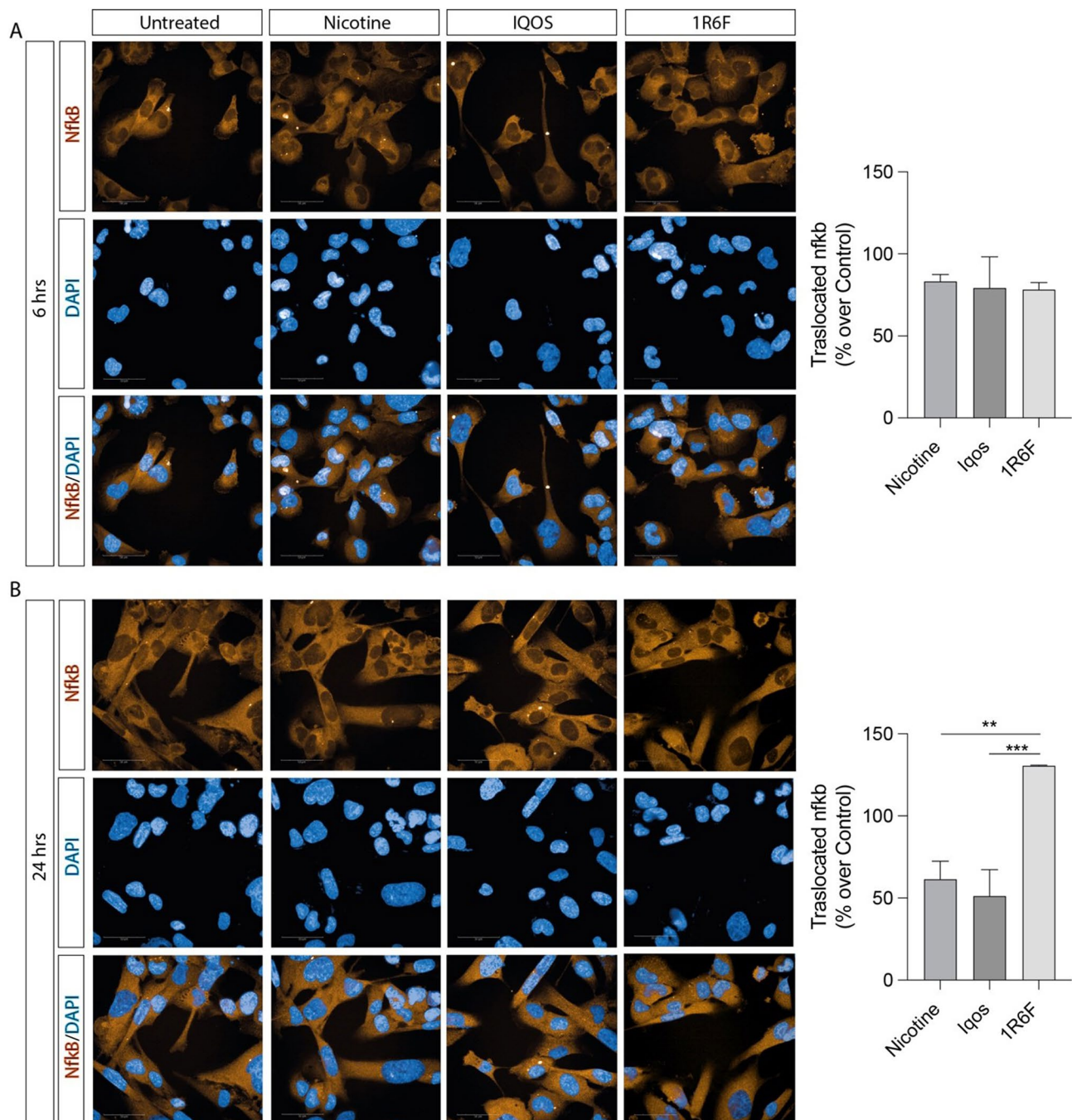
Fig. 8 Effect of cigarette smoke on NF-κB translocation. (**A**) Immunocytochemistry for NF-κB at 6 h. (**B**) Immunocytochemistry for NF-κB at 24 h. Values represent the mean ± SD of experiments performed in quadruplicate. (**$p \leq 0.01$, ***$p \leq 0.001$)

findings are coherent with previous reports showing that HTP results in a minimal impact on neurodegenerative disease and that the gene expression profile of cerebral cortex tissues does not involve inflammatory pathways [37]. In order to determine possible biochemical mechanisms responsible for the toxicological profiles, we also measured various markers of oxidative stress under our experimental conditions. These set of experiments

showed that cigarette exposure resulted in a significant increase of ROS, nitrosative stress, lipid peroxidation and a significant decrease of intracellular GSH levels. Interestingly, no significant effects on oxidative stress markers were observed in nicotine treated cells or after exposure to HTP. Our results are consistent with previous reports showing that [38] cigarettes induced the levels of peroxides, pro-inflammatory cytokine expression, autophagy,
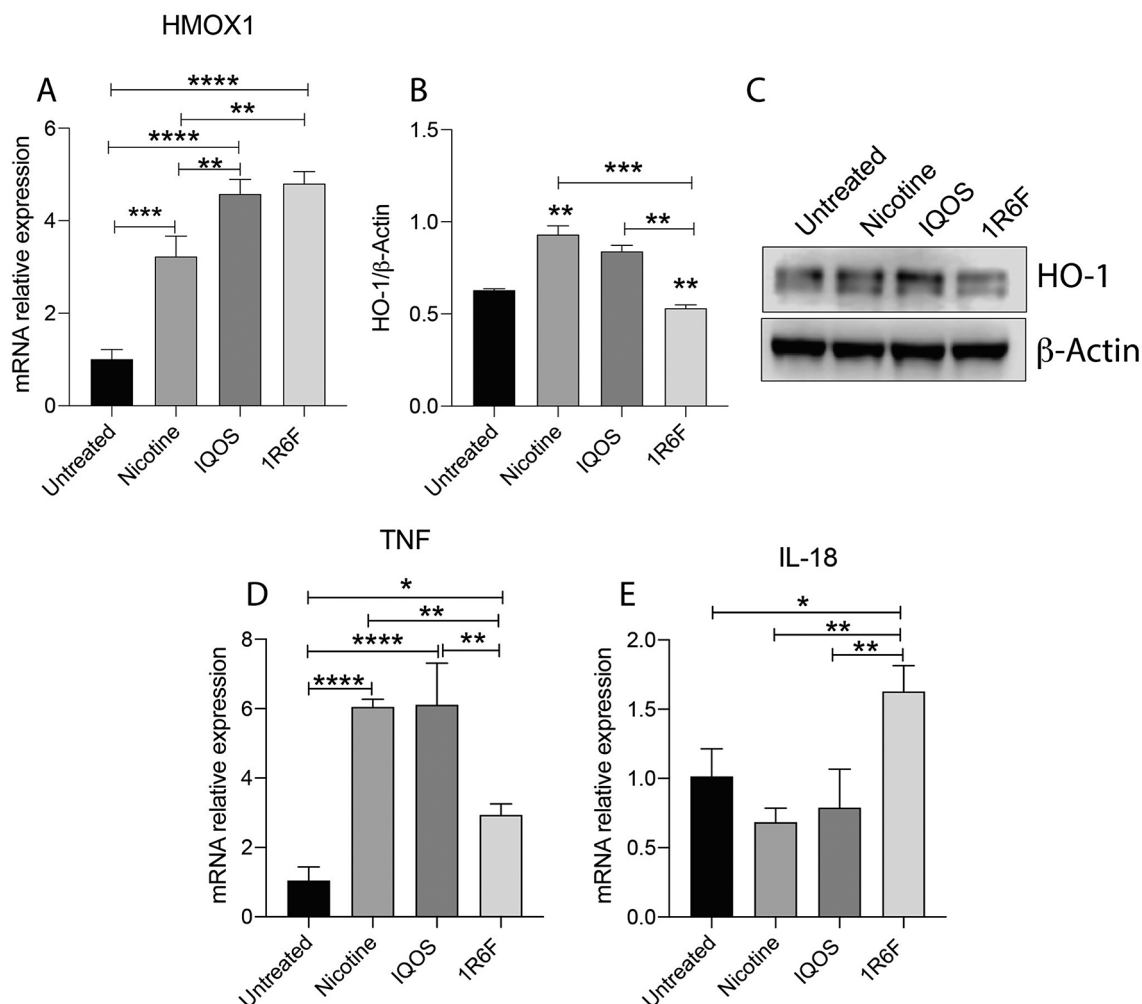
Fig. 9 Effect of cigarette smoke in inflammatory cytokines expression. mRNA expression levels of (**A**) HMOX1, (**D**) TNF, (**E**) IL-18. (**B**) Densitometry analysis of HMOX1. (**C**) Western blot analysis of HMOX1 protein. β-Actin protein was used as a total protein loading reference. Values represent the mean ± SD of experiments performed in quadruplicate. (*$p < 0.05$, **$p \leq 0.01$, ***$p \leq 0.001$, ****$p \leq 0.0001$)

catalytic Fe (II) and 8-hydroxy-2'-deoxyguanosine when compared to HTPs.

Further examination of mitochondrial dynamics reveals impairments in mitochondrial fission mechanisms, as evidenced by decreased DRP1 and increased mitofusins (MFN1 and MFN2) expression in HMC3 cells treated with 1R6F AqE. Given the crucial role of DRP1 and since many studies reported that DRP1 undergoes several post-translation modifications [39], future studies should explore potential associations between these modifications and mitochondrial dynamics imbalance.

Various stressors, including ROS, can lead to the accumulation of misfolded proteins detected by the unfolded protein response (URP). This is a signaling system that coordinates a cellular response aimed at restoring protein homeostasis [40]. There are three key regulators (IRE1α, PERK, ATF6) involved in UPR signal activation which give rise to separate branches of the response [41].

ER stress sensors activation is inhibited by physical interaction, in the ER lumen, with BIP which induces their allosteric changes [42]. BIP is a major ER chaperone which is able to switch from its chaperone cycle to ER stress sensor cycle [41]. Its distribution is also altered in several neurodegenerative diseases, in cancer and during infections [43]. Binding affinity analysis indicated that, in the absence of ER stress, IRE1α will be bound to BIP. This interaction favors BIP acting as a stress sensor. IRE1α is a low expression protein [44], while BIP is one of the most abundant proteins in the ER. This strong difference in concentration could protect cells from UPR activation at low levels of misfolded proteins [41].

In our work, we observed increased protein expression of BIP and decreased IRE1α protein levels in HMC3 1R6F AqE treated cells. Overexpression of BIP above the endogenous level significantly suppressed the activation of IRE1α [45].
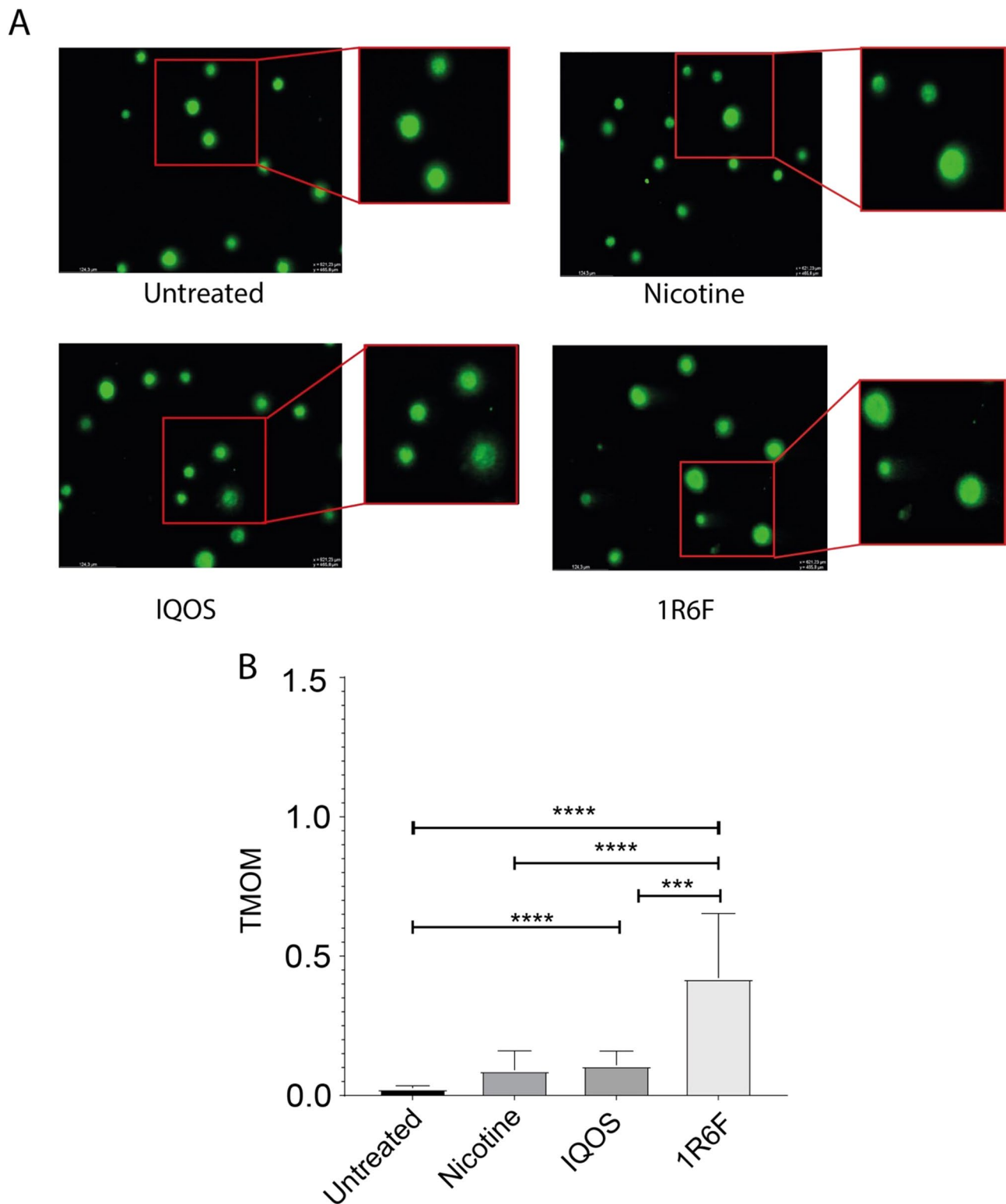
Fig. 10 DNA damage measured by the comet assay. HMC3 cells were exposed for 24 h to nicotine, IQOS and 1R6F. (**A**) Representative fluorescence images of comets. (**B**) DNA double strand breaks (DSBs) were measured by neutral comet assay and expressed as TMOM. Data presented are median of ±95% CI of experiments performed in quadruplicate. (*** $p \leq 0.001$ and ****$p \leq 0.0001$, as a result of the Kruskal-Wallis test followed by Dunnett's post hoc test, denotes a significant increase in DSBs as indicated by the brackets for each specific comparison)
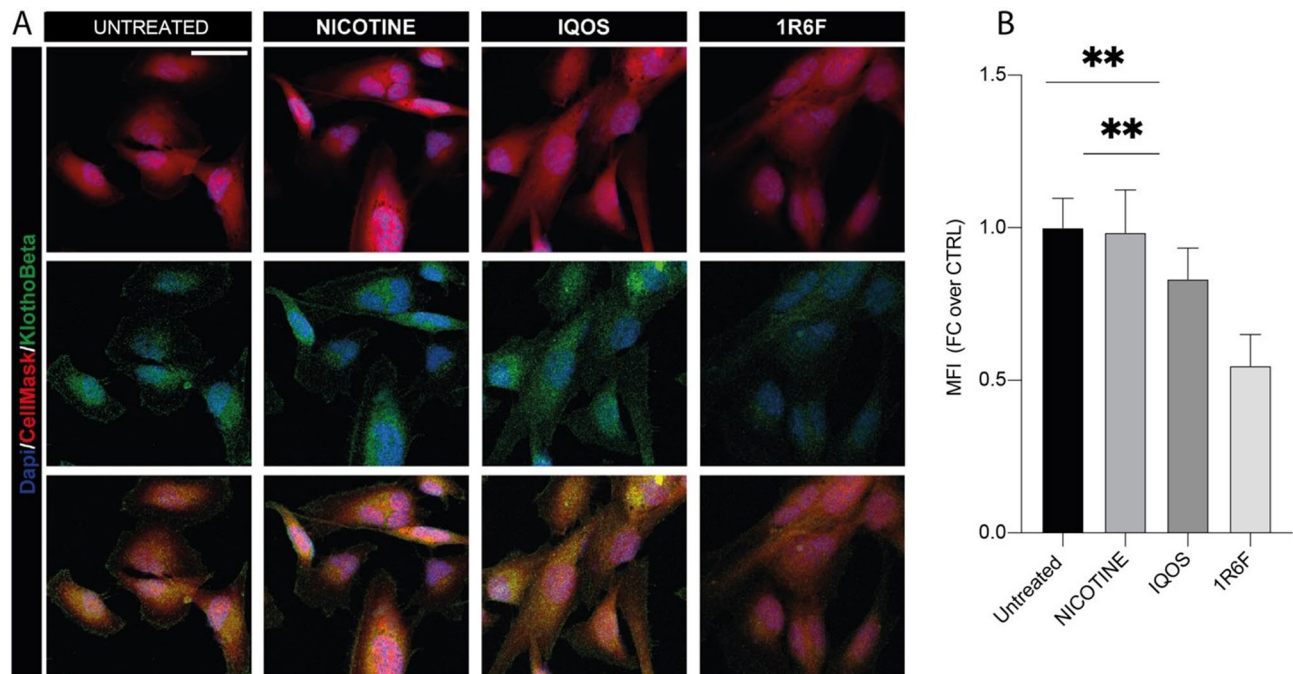
Fig. 11 Effect of cigarette smoke on Klotho β expression. (**A**, **B**) Immunofluorescence of Klotho β and CellMask. HMC3 cells were exposed for 24 h to nicotine, IQOS and 1R6F. Values represent the mean ± SD of experiments performed in quadruplicate. (**p ≤ 0.01). (Scale bars in (**A**) 50 μm)
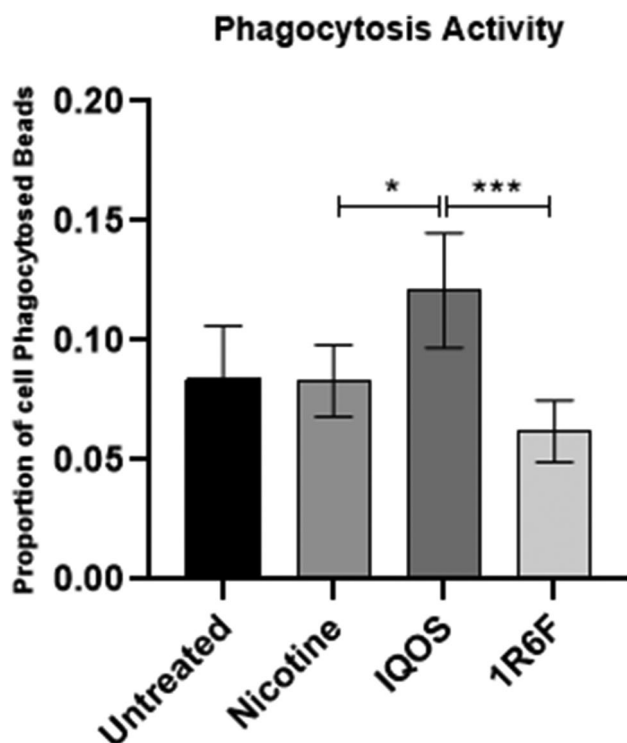

Fig. 12 Phagocytosis activity by beads. The height of the bars represents the calculated proportion using the Exact Method. The error bars stand for the 95% confidence interval of the proportion. (*p < 0.05, *** p ≤ 0.001)

We also noticed that, after all the three treatments PERK increased even though the cells overexpressed BIP.

This result implies that PERK is the most sensitive branch of the UPR signaling, which also may explain why it is not easily attenuated during ER stress conditions [45].

It is important to underline that UPR sensors are activated through dimerization and phosphorylation mechanisms [46], so in order to explore the link between the effects of cigarette smoke and UPR on HMC3 cells, it would be interesting to assess the phosphorylation status of these factors reflecting their full activation.

Moreover, our findings underscore the significance of Nuclear Factor Erythroid Related Factor 2 (Nrf2) and Nuclear Factor-kB (NF-kB) in the cellular response to oxidative stress and inflammation [47–49]. Dysregulation of these pathways can exacerbate oxidative damage and inflammation, potentially leading to apoptotic responses. A major pathway that maintains redox homeostasis in the brain is the transcription factor nuclear erythroid 2-related factor 2 (Nrf2), which binds to the antioxidant response element (ARE) located at the promoter region of antioxidant genes [50, 51]. Nrf2 is ubiquitously expressed in the brain and plays a crucial role in defense mechanism against oxidative stress toxicity [52]. In addition to its antioxidant activities, Nrf2 is an anti-inflammatory agent by inhibiting NF-kB activities. Moreover, the activation of the transcription factor NF-kB, is suggested to be the primary regulation for inflammatory responses [53]. NF-kB is responsible for proinflammatory

Table 2 Summary of HMC3 cells phagocytosis assay results. Human microglial cell line, HMC3, was treated by 4 treatments: untreated (control), nicotine, 1R6F, or IQOS. The total number of cells from 5 random fields was tabulated in the table. The number of cells that have phagocytosis fluorescent beads was also presented. The observed proportion was calculated using cell phagocytosis fluorescent beads divided by the total number of cells. For each observed proportion, the confidence interval (exact method) at a 95% confidence level, the calculated proportion, and the margin of error were computed and summarized in this table

Treatments	Total number of cells	Total cell count poisson confidence Interval (95%)	Total Number of cells phagocytosed fluorescent beads	Observed Proportion (p) of cells with beads	Calculated Proportion (p')	Margin of Error (w)	95% confidence interval (exact method)
Untreated	651	[602.703]	55	0.084	0.086	0.022	[0.064, 0.109]
Nicotine	1329	[1259,1402]	110	0.083	0.084	0.015	[0.069, 0.099]
IQOS	743	[691.798]	90	0.121	0.123	0.024	[0.099,0.147]
1R6F	1337	[1266.1411]	83	0.062	0.063	0.013	[0.050, 0.076]

Table 3 Odds ratios and p-values. The odds ratio (OR) of phagocytosed cells from various treatments is reported in this table. Fisher's exact tests were used to calculate the p-values with the null hypothesis as OR = 1. The false discovery rate (FDR) method has been used to minimize the type I error accumulated from the 6 comparisons and adjust the p-values

A vs. B	Odds ratio (odd of B/odd of A)	Raw *p*-value from fisher's exact test	FDR corrected *p*-value (q-value)
Untreated vs. Nicotine	0.9796805	0.9313	0.9313
Untreated vs. 1R6F	0.7348761	0.09265	0.11118
Untreated vs. IQOS	1.43341	0.04444	0.08888
Nicotine vs. 1R6F	0.7501089	0.06219	0.093285
Nicotine vs. IQOS	1.463162	0.01126	0.03378
1R6F vs. IQOS	1.950662	3.66E-05	0.0002196

gene induction, which increases inflammatory response [54]. Furthermore, the increase in NF-kB expression can also lead to a further decrease in Nrf2 [55], confirmed also by our findings.

Changes in the redox state within the cell can alter the regulation of intracellular signaling, chromatin remodeling, and activation of redox-sensitive transcription factors, such as NF-kB, linking cigarette smoke exposure to altered cytokine production. Cigarette smoke therefore promotes inflammation by inducing the production of pro-inflammatory cytokines [56].

It has been suggested that the Nrf2/ARE pathway plays a crucial role in regulating the intracellular redox state, and oxidative stress is one of the most potent stimuli for its activation. Consistently, our data suggest that exposure to cigarette smoke results in a time dependent impairment of Nrf2/ARE pathway response to intracellular oxidative stress. These results are consistent with previous clinical studies showing reduced Nrf2 expression in whole lung tissue and alveolar macrophages of patients with pulmonary emphysema [29], as well as in pulmonary macrophages of current smokers and patients with chronic obstructive pulmonary disease (COPD) [30], conditions where oxidant-antioxidant imbalance is strongly implicated [32, 33]. Additionally, our study

demonstrates that, unlike the Nrf2/ARE pathway, there was a progressive activation of NF-kB in HMC3 following cigarette smoke exposure compared to untreated cells. A substantial body of experimental evidence supports the activation of the transcription factor NF-kB as a key redox-sensitive event linked to neuroinflammation (PMID: PMID: 38259497). The reasons for this unexpected result on Nrf2 are unclear. Recent data have shown that NF-kB p65 subunit repressed the Nrf2/ARE pathway at transcriptional level [17]. In particular, in the cells where NF-kB and Nrf2 were simultaneously activated, p65 unidirectionally antagonized the transcriptional activity of Nrf2.

Microglia also play an important role in the inflammatory process in the central nervous system [57]. Our findings show that the treatment of HMC3 cells with 1R6F induces an increase in IL-18.

In order to further understand the interplay of smoking and HMC3 cells, we employed the neutral comet assay to measure double strand DNA damage. The principle of that assay is based on alterations found in DNA such as strand breaks resulting in the extension of DNA loops from lysed and salt-extracted nuclei, which, in turn, form a comet-like tail after either alkaline electrophoresis, indicating SSBs, or neutral electrophoresis, indicating DSBs. In previous studies in which the effects of cigarette smoke condensate/cigarette smoke on DNA strand breaks were investigated by the comet assay, only DNA single-strand breaks were detected [58].

The interaction of cigarette smoke treatment in a clinically relevant dose on DNA DSBs in HMC3 cells has not been reported previously. The increase in TMOM observed upon combustible cigarette exposure is associated with a slight double-stranded damage.

To evaluate the effects on aging in HMC3 cells we have studied the role of Klotho β. This is a protein that when under-expressed, in mice, causes a syndrome of aging, including a short lifespan [59]. Although all the roles of Klotho β in the CNS are not yet fully understood, it may play an important role in neuroprotection. A reduction of this protein is associated with nerve damage and

brain dysfunction [60]. Our findings reveal that cigarette smoke leads to a decrease in the protein expression of Klotho β suggesting an attenuation in its neuroprotective role, promoting aging.

Microglial phagocytosis of pathogens, extracellular protein aggregates, and apoptotic cell debris dampens inflammation, protects neurons and keeps homeostasis in the CNS. Deficient or excessive microglial phagocytic ability could lead to abnormal synaptic connections and deposits of aggregated proteins [32]. Our findings showed a lower phagocytic ability of HMC3 cells treated with cigarette smoke. We suppose that this is due to the inflammatory state triggered by cigarette exposure which leads to a depletion of the cells' phagocytic ability.

Our results give valuable insights into the implications of cigarette smoking in neuroinflammation and/or neurodegeneration and may provide a possible rationale to develop harm reduction strategies for heavy smokers.

Conclusion

This study further demonstrates that HTP exhibits reduced toxicity in microglial cells when compared to cigarette smoke using ISO standard and clinically relevant conditions of exposure. In particular, HTP showed reduced oxidative stress and inflammation compared to cigarette smoke which in turs leads to increased microglial dysfunction and senescence. Furthermore, nicotine does not appear to be directly responsible for the deleterious effects of cigarette smoke on microglial cells. Future studies are now warranted in order to translate such effects into an in vivo setting with particular regard to chronic conditions of exposure.

Our study concluded that HTP and nicotine resulted in a significant reduction of toxicity when compared to cigarette smoke even though they should not be considered risk free products. Some limitations of the study should be taken into due account in order to further validate our results. In particular, our study was conducted using HMC3 in a controlled laboratory environment, which may not fully replicate the complex biological responses of the human brain in vivo. The findings may differ in living organisms due to factors such as metabolic interactions, blood-brain barrier dynamics, and long-term exposure effects. Furthermore, the experiments primarily examined the effects of short-term (acute) exposure to cigarette smoke and HTP aerosol. Chronic exposure over longer periods may produce different toxicological and inflammatory responses, which this study did not address. Finally, The findings are based solely on cell-based experiments and have not been validated in animal models or human clinical trials. This limits the ability to make direct conclusions about the effects of cigarette smoke or HTPs on brain health in living organisms.

Abbreviations

AqE	Aqueous Extract
ENDS	Electronic nicotine delivery systems
HTPs	Heating tobacco products
E-cigs	Electronic Cigarettes
HCS	High Content Screening
ISO	International Organization for Standardization
HCI	Health Canada Intensive
CRM81	CORESTA Recommended Method n. 81
BAX	Bcl-2-associated X protein
BIP	Binding Immunoglobulin Protein
CLPP	Caseinolytic protease P
ER	Endoplasmic reticulum
GSH	Glutathione
HSP60	Heat shock protein 60
HSP90	Heat shock protein 90
IRE1α	Inositol requiring enzyme 1

Data availability
All data and material will be available upon request to the corresponding author.

Declarations

Ethics approval and consent to participate
Not applicable.

Consent for publication
All the authors consent for publication of this manuscript in its present form,

Conflict of interest
The authors declare no conflict of interest.

Author details
[1]Department of Biomedical and Biotechnological Sciences, University of Catania, Via S. Sofia, 97, Catania 95123, Italy
[2]Department of Clinical and Experimental Medicine, University of Catania, Via S. Sofia, 89, Catania 95123, Italy
[3]Center of Excellence for the Acceleration of Harm Reduction (CoEHAR), University of Catania, Via S. Sofia, 97, Catania 95123, Italy
[4]Department of Biology, College of Science and Technology, Temple University, Philadelphia, PA 19122, USA
[5]Sbarro Institute for Cancer Research and Molecular Medicine, Center for Biotechnology, College of Science and Technology, Temple University, Philadelphia, PA 19122, USA
[6]Department of Drug and Health Science, Section of Biochemistry, University of Catania, Catania 95125, Italy

[7]Pharmaceutical Biotechnology Laboratory, Department of Pharmaceutical Chemistry, College of Pharmacy, King Saud University, Riyadh 11451, Saudi Arabia

References

1. Mathers CD, Loncar D. Projections of global mortality and burden of disease from 2002 to 2030. PLoS Med. 2006;3:e442.
2. Loboda A, Damulewicz M, Pyza E, Jozkowicz A, Dulak J. Role of Nrf2/HO-1 system in development, oxidative stress response and diseases: an evolutionarily conserved mechanism. Cell Mol Life Sci. 2016;73:3221–47.
3. Pirie K, Peto R, Reeves GK, Green J, Beral V, Million Women Study C. The 21st century hazards of smoking and benefits of stopping: a prospective study of one million women in the UK. Lancet. 2013;381:133–41.
4. Moylan S, Jacka FN, Pasco JA, Berk M. How cigarette smoking may increase the risk of anxiety symptoms and anxiety disorders: a critical review of biological pathways. Brain Behav. 2013;3:302–26.
5. Durazzo TC, Mattsson N, Weiner MW. Alzheimer's Disease Neuroimaging I: smoking and increased Alzheimer's disease risk: a review of potential mechanisms. Alzheimers Dement. 2014;10:S122–145.
6. Mazzone P, Tierney W, Hossain M, Puvenna V, Janigro D, Cucullo L. Pathophysiological impact of cigarette smoke exposure on the cerebrovascular system with a focus on the blood-brain barrier: expanding the awareness of smoking toxicity in an underappreciated area. Int J Environ Res Public Health. 2010;7:4111–26.
7. Zhong G, Wang Y, Zhang Y, Guo JJ, Zhao Y. Smoking is associated with an increased risk of dementia: a meta-analysis of prospective cohort studies with investigation of potential effect modifiers. PLoS ONE. 2015;10:e0118333.
8. Mappin-Kasirer B, Pan H, Lewington S, Kizza J, Gray R, Clarke R, Peto R. Tobacco smoking and the risk of Parkinson disease: a 65-year follow-up of 30,000 male British doctors. Neurology. 2020;94:e2132–8.
9. Wang C, Zhou C, Guo T, Huang P, Xu X, Zhang M. Association between cigarette smoking and Parkinson's disease: a neuroimaging study. Ther Adv Neurol Disord. 2022;15:17562864221092566.
10. Henningfield JE, Fant RV. Tobacco use as drug addiction: the scientific foundation. Nicotine Tob Res. 1999;1(Suppl 2):S31–35.
11. In The Health Consequences of Smoking-50 Years of Progress: A Report of the Surgeon General. Atlanta (GA); 2014: Reports of the Surgeon General].
12. Samet JM. Epidemiology and the Tobacco Epidemic: how Research on Tobacco and Health shaped epidemiology. Am J Epidemiol. 2016;183:394–402.
13. Yan F, Gao H, Zhao H, Bhatia M, Zeng Y. Roles of airway smooth muscle dysfunction in chronic obstructive pulmonary disease. J Transl Med. 2018;16:262.
14. Liu X, Chen Z. The pathophysiological role of mitochondrial oxidative stress in lung diseases. J Transl Med. 2017;15:207.
15. Ho YS, Yang X, Yeung SC, Chiu K, Lau CF, Tsang AW, Mak JC, Chang RC. Cigarette smoking accelerated brain aging and induced pre-alzheimer-like neuropathology in rats. PLoS ONE. 2012;7:e36752.
16. G SB, Choi S, Krishnan J, K R. Cigarette smoke and related risk factors in neurological disorders: an update. Biomed Pharmacother. 2017;85:79–86.
17. Cigarette smoking machine. - HAUNI LM series [https://www.directindustry.com/prod/koerber-technologies-gmbh/product-116079-2468335.html]
18. ISO 3402:. 2023 - Tobacco and tobacco products — Atmosphere for conditioning and testing [https://www.iso.org/standard/83089.html]
19. ISO/TR 19478-2. 2015(en) ISO and Health Canada intense smoking parameters [https://www.iso.org/obp/ui/#iso:std:iso:tr:19478:-2:ed-1:v1:en].
20. Adamson J, Jaunky T, Thorne D, Gaca MD. Characterisation of the borgwaldt LM4E system for in vitro exposures to undiluted aerosols from next generation tobacco and nicotine products (NGPs). Food Chem Toxicol. 2018;113:337–44.
21. Panda ASPK, Shivakumar HN, Repka MA, Murthy SN. Nicotine loaded dissolving microneedles for nicotine replacement therapy. J Drug Deliv Sci Technol. 2021;61:102300.
22. Caruso M, Distefano A, Emma R, Zuccarello P, Copat C, Ferrante M, Carota G, Pulvirenti R, Polosa R, Missale GA, et al. In vitro cytoxicity profile of e-cigarette liquid samples on primary human bronchial epithelial cells. Drug Test Anal. 2023;15:1145–55.
23. Chazotte B. Labeling mitochondria with MitoTracker dyes. Cold Spring Harb Protoc. 2011;2011:990–2.
24. Tran TP, Tu H, Liu J, Muelleman RL, Li YL. Mitochondria-derived superoxide links to tourniquet-induced apoptosis in mouse skeletal muscle. PLoS ONE. 2012;7:e43410.
25. Tomasello B, Grasso S, Malfa G, Stella S, Favetta M, Renis M. Double-face activity of resveratrol in voluntary runners: assessment of DNA damage by comet assay. J Med Food. 2012;15:441–7.
26. Barone R, Macaluso F, Sangiorgi C, Campanella C, Marino Gammazza A, Moresi V, Coletti D, Conway de Macario E, Macario AJ, Cappello F, et al. Skeletal muscle heat shock protein 60 increases after endurance training and induces peroxisome proliferator-activated receptor gamma coactivator 1 alpha1 expression. Sci Rep. 2016;6:19781.
27. Marino Gammazza A, Campanella C, Barone R, Caruso Bavisotto C, Gorska M, Wozniak M, Carini F, Cappello F, D'Anneo A, Lauricella M, et al. Doxorubicin anti-tumor mechanisms include Hsp60 post-translational modifications leading to the Hsp60/p53 complex dissociation and instauration of replicative senescence. Cancer Lett. 2017;385:75–86.
28. Lazzarino G, Amorini AM, Fazzina G, Vagnozzi R, Signoretti S, Donzelli S, Di Stasio E, Giardina B, Tavazzi B. Single-sample preparation for simultaneous cellular redox and energy state determination. Anal Biochem. 2003;322:51–9.
29. Romitelli F, Santini SA, Chierici E, Pitocco D, Tavazzi B, Amorini AM, Lazzarino G, Di Stasio E. Comparison of nitrite/nitrate concentration in human plasma and serum samples measured by the enzymatic batch Griess assay, ion-pairing HPLC and ion-trap GC-MS: the importance of a correct removal of proteins in the Griess assay. J Chromatogr B Analyt Technol Biomed Life Sci. 2007;851:257–67.
30. Tibullo D, Giallongo C, Romano A, Vicario N, Barbato A, Puglisi F, Parenti R, Amorini AM, Wissam Saab M, Tavazzi B et al. Mitochondrial functions, Energy Metabolism and protein glycosylation are interconnected processes mediating resistance to Bortezomib in multiple myeloma cells. Biomolecules. 2020;10(5):696. https://doi.org/10.3390/biom10050696.
31. Longhitano L, Distefano A, Musso N, Bonacci P, Orlando L, Giallongo S, Tibullo D, Denaro S, Lazzarino G, Ferrigno J, et al. (+)-Lipoic acid reduces mitochondrial unfolded protein response and attenuates oxidative stress and aging in an in vitro model of non-alcoholic fatty liver disease. J Transl Med. 2024;22:82.
32. Lian H, Roy E, Zheng H. Microglial phagocytosis assay. Bio Protoc. 2016;6(21):e1988. https://doi.org/10.21769/BioProtoc.1988.
33. Macaluso M, Caracciolo V, Rizzo V, Sun A, Montanari M, Russo G, Bellipanni G, Khalili K, Giordano A. Integrating role of T antigen, Rb2/p130, CTCF and BORIS in mediating non-canonical endoplasmic reticulum-dependent death pathways triggered by chronic ER stress in mouse medulloblastoma. Cell Cycle. 2012;11:1841–50.
34. Xu X, Gao W, Li L, Hao J, Yang B, Wang T, Li L, Bai X, Li F, Ren H, et al. Annexin A1 protects against cerebral ischemia-reperfusion injury by modulating microglia/macrophage polarization via FPR2/ALX-dependent AMPK-mTOR pathway. J Neuroinflammation. 2021;18:119.
35. Schindelin J, Arganda-Carreras I, Frise E, Kaynig V, Longair M, Pietzsch T, Preibisch S, Rueden C, Saalfeld S, Schmid B, et al. Fiji: an open-source platform for biological-image analysis. Nat Methods. 2012;9:676–82.
36. Liu X, Jiang N, Zhou W. Various energetic metabolism of Microglia in response to different stimulations. Molecules 2023;28(11):4501. https://doi.org/10.21769/BioProtoc.1988.
37. Yamada H, Yamazaki Y, Takebayashi Y, Yazawa K, Sasanishi M, Motoda A, Nakamori M, Morino H, Takahashi T, Maruyama H. The long-term effects of heated tobacco product exposure on the central nervous system in a mouse model of prodromal Alzheimer's disease. Sci Rep. 2024;14:227.
38. Lyu Q, Jiang L, Zheng H, Hayashi S, Sato K, Toyokuni S. Diluted aqueous extract of heat-not-burn tobacco product smoke causes less oxidative damage in fibroblasts than conventional cigarette. J Clin Biochem Nutr. 2022;71:55–63.
39. Kraus F, Roy K, Pucadyil TJ, Ryan MT. Function and regulation of the divisome for mitochondrial fission. Nature. 2021;590:57–66.
40. Reverendo M, Mendes A, Arguello RJ, Gatti E, Pierre P. At the crossway of ER-stress and proinflammatory responses. FEBS J. 2019;286:297–310.
41. Kopp MC, Larburu N, Durairaj V, Adams CJ, Ali MMU. UPR proteins IRE1 and PERK switch BiP from chaperone to ER stress sensor. Nat Struct Mol Biol. 2019;26:1053–62.
42. Stagnitti MN. Trends in antidepressant utilization and expenditures in the U.S. Civilian Noninstitutionalized Population by Age, 2000 and 2010. Statistical brief (Medical Expenditure Panel Survey (US)). Rockville (MD); 2001.

43. Li W, Cao T, Luo C, Cai J, Zhou X, Xiao X, Liu S. Crosstalk between ER stress, NLRP3 inflammasome, and inflammation. Appl Microbiol Biotechnol. 2020;104:6129–40.

44. Boisvert FM, Ahmad Y, Gierlinski M, Charriere F, Lamont D, Scott M, Barton G, Lamond AI. A quantitative spatial proteomics analysis of proteome turnover in human cells. Mol Cell Proteom. 2012;11:M111011429.

45. Sundaram A, Appathurai S, Plumb R, Mariappan M. Dynamic changes in complexes of IRE1alpha, PERK, and ATF6alpha during endoplasmic reticulum stress. Mol Biol Cell. 2018;29:1376–88.

46. Hetz C. The unfolded protein response: controlling cell fate decisions under ER stress and beyond. Nat Rev Mol Cell Biol. 2012;13:89–102.

47. Fei L, Jingyuan X, Fangte L, Huijun D, Liu Y, Ren J, Jinyuan L, Linghui P. Pre-conditioning with rHMGB1 ameliorates lung ischemia-reperfusion injury by inhibiting alveolar macrophage pyroptosis via the Keap1/Nrf2/HO-1 signaling pathway. J Transl Med. 2020;18:301.

48. Peng J, Tang R, He J, Yu Q, Wang D, Qi D. S1PR3 inhibition protects against LPS-induced ARDS by inhibiting NF-kappaB and improving mitochondrial oxidative phosphorylation. J Transl Med. 2024;22:535.

49. Sun Z, Ji Z, Meng H, He W, Li B, Pan X, Zhou Y, Yu G. Lactate facilitated mitochondrial fission-derived ROS to promote pulmonary fibrosis via ERK/DRP-1 signaling. J Transl Med. 2024;22:479.

50. Itoh K, Chiba T, Takahashi S, Ishii T, Igarashi K, Katoh Y, Oyake T, Hayashi N, Satoh K, Hatayama I, et al. An Nrf2/small Maf heterodimer mediates the induction of phase II detoxifying enzyme genes through antioxidant response elements. Biochem Biophys Res Commun. 1997;236:313–22.

51. Motohashi H, Yamamoto M. Nrf2-Keap1 defines a physiologically important stress response mechanism. Trends Mol Med. 2004;10:549–57.

52. Kobayashi A, Kang MI, Watai Y, Tong KI, Shibata T, Uchida K, Yamamoto M. Oxidative and electrophilic stresses activate Nrf2 through inhibition of ubiquitination activity of Keap1. Mol Cell Biol. 2006;26:221–9.

53. Hayden MS, West AP, Ghosh S. NF-kappaB and the immune response. Oncogene. 2006;25:6758–80.

54. Zhang T, Ma C, Zhang Z, Zhang H, Hu H. NF-kappaB signaling in inflammation and cancer. MedComm (2020) 2021, 2:618–653.

55. Davinelli S, Saso L, D'Angeli F, Calabrese V, Intrieri M, Scapagnini G. Astaxanthin as a modulator of Nrf2, NF-kappaB, and their crosstalk: Molecular mechanisms and possible clinical applications. Molecules. 2022;27(2):502. https://doi.org/10.3390/molecules27020502.

56. Strzelak A, Ratajczak A, Adamiec A, Feleszko W. Tobacco smoke induces and alters Immune responses in the lung triggering inflammation, Allergy, Asthma and other Lung diseases: a mechanistic review. Int J Environ Res Public Health. 2018;15(5):1033. https://doi.org/10.3390/ijerph15051033.

57. Na KS, Jung HY, Kim YK. The role of pro-inflammatory cytokines in the neuro-inflammation and neurogenesis of schizophrenia. Prog Neuropsychopharmacol Biol Psychiatry. 2014;48:277–86.

58. Moktar A, Ravoori S, Vadhanam MV, Gairola CG, Gupta RC. Cigarette smoke-induced DNA damage and repair detected by the comet assay in HPV-transformed cervical cells. Int J Oncol. 2009;35:1297–304.

59. Sun H, Gao Y, Lu K, Zhao G, Li X, Li Z, Chang H. Overexpression of Klotho suppresses liver cancer progression and induces cell apoptosis by negatively regulating wnt/beta-catenin signaling pathway. World J Surg Oncol. 2015;13:307.

60. Ranjbar N, Raeisi M, Barzegar M, Ghorbanihaghjo A, Shiva S, Sadeghvand S, Negargar S, Poursistany H, Raeisi S. The possible anti-seizure properties of Klotho. Brain Res. 2023;1820:148555.

Publisher's note